



# **NiONPs-induced alteration in calcium signaling and mitochondrial function in pulmonary artery endothelial cells involves oxidative stress and TRPV4 channels disruption**

Ophélie Germande, Magalie Baudrimont, Fabien Beaufiles, Véronique Freund-Michel, Thomas Ducret, Jean-François Quignard, Marie-Hélène Errera, Sabrina Lacomme, Etienne Gontier, Stéphane Mornet, et al.

## **► To cite this version:**

Ophélie Germande, Magalie Baudrimont, Fabien Beaufiles, Véronique Freund-Michel, Thomas Ducret, et al.. NiONPs-induced alteration in calcium signaling and mitochondrial function in pulmonary artery endothelial cells involves oxidative stress and TRPV4 channels disruption. *Nanotoxicology*, 2022, 16 (1), pp.29-51. 10.1080/17435390.2022.2030821 . hal-03675998

**HAL Id: hal-03675998**


**<https://hal.science/hal-03675998>**

Submitted on 29 Jun 2022

**HAL** is a multi-disciplinary open access archive for the deposit and dissemination of scientific research documents, whether they are published or not. The documents may come from teaching and research institutions in France or abroad, or from public or private research centers.

L'archive ouverte pluridisciplinaire **HAL**, est destinée au dépôt et à la diffusion de documents scientifiques de niveau recherche, publiés ou non, émanant des établissements d'enseignement et de recherche français ou étrangers, des laboratoires publics ou privés.

# NiONPs-induced alteration in calcium signaling and mitochondrial function in pulmonary artery endothelial cells involves oxidative stress and TRPV4 channels disruption

Ophélie Germande<sup>a,b,c</sup>, Magalie Baudrimont<sup>a,c</sup> , Fabien Beaufiglioli<sup>a,b,d</sup>, Véronique Freund-Michel<sup>a,b</sup>, Thomas Ducret<sup>a,b</sup>, Jean-François Quignard<sup>a,b</sup>, Marie-Hélène Errera<sup>e</sup>, Sabrina Lacomme<sup>a,f</sup>, Etienne Gontier<sup>a,f</sup>, Stéphane Mornet<sup>g</sup>, Megi Bejko<sup>g</sup>, Bernard Muller<sup>a,b</sup>, Roger Marthan<sup>a,b,d</sup>, Christelle Guibert<sup>b</sup>, Juliette Deweirdt<sup>a,b,\*</sup> and Isabelle Baudrimont<sup>a,b,\*</sup>

<sup>a</sup>Université de Bordeaux, Bordeaux, France; <sup>b</sup>INSERM U 1045, Centre de Recherche Cardio-Thoracique, Pessac, France; <sup>c</sup>UMR EPOC 5805, Université de Bordeaux, Arcachon, France; <sup>d</sup>Service d'Exploration Fonctionnelle Respiratoire, Service de Pédiatrie Médicale, CHU de Bordeaux, Bordeaux, France; <sup>e</sup>Department of Ophthalmology, University of Pittsburgh School of Medicine, Pittsburgh, PA, USA;

<sup>f</sup>CNRS, INSERM, BIC, UMS 3420, Université de Bordeaux, Bordeaux, France; <sup>g</sup>CNRS Bordeaux INP, ICMCB, UMR 5026, Université de Bordeaux, Bordeaux, France

## ABSTRACT

In New Caledonia, anthropic activities, such as mining, increase the natural erosion of soils in nickel mines, which in turn, releases nickel oxide nanoparticles (NiONPs) into the atmosphere. Pulmonary vascular endothelial cells represent one of the primary targets for inhaled nanoparticles. The objective of this *in vitro* study was to assess the cytotoxic effects of NiONPs on human pulmonary artery endothelial cells (HPAEC). Special attention will be given to the level of oxidative stress and calcium signaling, which are involved in the physiopathology of cardiovascular diseases. HPAEC were exposed to NiONPs (0.5–150 µg/cm<sup>2</sup>) for 4 or 24 h. The following different endpoints were studied: (i) ROS production using CM-H<sub>2</sub>DCF-DA probe, electron spin resonance, and MitoSOX probe; the SOD activity was also measured (ii) calcium signaling with Fluo4-AM, Rhod-2, and Fluo4-FF probes; (iii) inflammation by IL-6 production and secretion and, (iv) mitochondrial dysfunction and apoptosis with TMRM and MitoTracker probes, and AnnexinV/PI. Our results have evidenced that NiONPs induced oxidative stress in HPAEC. This was demonstrated by an increase in ROS production and a decrease in SOD activity, the two mechanisms seem to trigger a pro-inflammatory response with IL-6 secretion. In addition, NiONPs exposure altered calcium homeostasis inducing an increased cytosolic calcium concentration ([Ca<sup>2+</sup>]<sub>i</sub>) that was significantly reduced by the extracellular calcium chelator EGTA and the TRPV4 inhibitor HC-067047. Interestingly, exposure to NiONPs also altered TRPV4 activity. Finally, HPAEC exposure to NiONPs increased intracellular levels of both ROS and calcium ([Ca<sup>2+</sup>]<sub>m</sub>) in mitochondria, leading to mitochondrial dysfunction and HPAEC apoptosis.

## KEYWORDS

Nickel oxide nanoparticles (NiONPs); pulmonary endothelial cells; reactive oxygen species; calcium signaling; mitochondrial dysfunction

## Introduction

New Caledonia is one of the largest nickel producers in the world, producing about 158 000 tons of nickel per year. The mineral resources are concentrated in ultramafic formations covering nearly 30% of the New Caledonian subsoils (Isnard et al. 2016). Ultramafic soils are characterized by a high concentration of trace elements including nickel (Ni), chromium (Cr), cobalt (Co), and manganese (Mn) (Losfeld et al. 2015). Soil erosion releases particles into the atmosphere, such as Ni particles. The

emission of atmospheric particles is amplified by an increased erosion of ultramafic soils, due to anthropic activities, such as mining (He, Yang, and Stoffella 2005; Pasquet et al. 2016) increasing the release of ultrafine particles (UFPs). They are called nanoparticles (NPs) once manufactured. Anthropogenic activities are, in turn, favored by the industry with the current development of nanotechnologies. The hydrometallurgical process contributes to Ni UFPs oxidation that mostly generates nickel oxide in redox state +II (NiO<sup>2+</sup>) (Yokel, Lasley, and Dorman

**CONTACT** Isabelle Baudrimont  [isabelle.baudrimont@u-bordeaux.fr](mailto:isabelle.baudrimont@u-bordeaux.fr)  Université de Bordeaux, 146, rue Léo Saignat, Bordeaux F-33076, France; INSERM U 1045, Centre de Recherche Cardio-Thoracique, Pessac, France

\*Co-last authors.

2006). Thereafter, NiO nanoparticles (NiONPs) can be used in many areas of industry, such as catalysts, energy storage devices, or lithium-ion batteries (especially for electric cars) (Imran Din and Rani 2016).

However, this increased use of NiONPs may contribute to anthropic emission of particles increase and hence increase the risk of particle inhalation by workers and surrounding populations. This leads to a public health concern. Some recent studies revealed significant contamination of the populations of New Caledonia because of soil enrichment by this metal (St-Jean et al. 2018). Moreover, it has been shown that nickel refinery workers had elevated nickel levels in lung tissues (Andersen and Svenes 1989) and that cardiovascular diseases were more prevalent among those workers (Norseth 1994). Thus, it is crucial to evaluate the potentially toxic effects of NiONPs due to the significant increase of anthropic emissions and the variety of their application. In particular, the workers and surrounding populations must have to undergo a risk assessment.

NiONPs are mainly composed of metal elements. They are potentially more harmful than larger-sized particles because of their high surface reactivity, their physical properties, and their large surface area leading to greater interactions with biological systems (Oberdorster, Oberdorster, and Oberdorster 2005). After inhalation, NPs deposition in the lungs is greater than larger-sized particles ( $>1\ \mu\text{m}$ ), because NPs are able to accumulate in lung alveoli and in lung parenchyma near the pulmonary arteries (Horemans et al. 2012). Compared to larger-sized particles, NPs can efficiently cross the pulmonary epithelial barrier to reach the pulmonary circulation, where they can be in direct contact with endothelial cells (ECs) that line the inner surface of arteries (Miller et al. 2017). Nemmar et al. (2002), have demonstrated that inhaled NPs can translocate from the lung into the blood. Therefore, NPs likely interact with ECs. ECs play a major role in vascular diseases because they are involved in vascular tone regulation, coagulation control, and vascular barrier integrity (Sandow et al. 2012). Previous *in vivo* studies have evaluated the pulmonary toxicity of NiONPs after intra-tracheal installation in rodents (Wistar rats and mice). NiONPs exposure resulted in pulmonary inflammation characterized by alveolar

proteinosis and a significant increase in neutrophils, eosinophils, macrophages, and lymphocytes and in pulmonary fibrosis (Senoh et al. 2017; Chang et al. 2017; Mo et al. 2019).

Other *in vitro* studies have demonstrated that NiONPs cause oxidative stress and calcium signaling alterations. Both are critical events involved in the physiopathology of cardiovascular diseases such as pulmonary hypertension (PH) (Guibert, Marthan, and Savineau 2007; Lai, Lu, and Wang 2015). Oxidative stress has been identified as the common mechanism of cellular damage after exposure to NPs (Deweirdt et al. 2020). The number of reactive oxygen species (ROS) generated was higher than exposure to larger particles, likely due to NPs higher surface area (Sioutas, Delfino, and Singh 2005). As regards calcium signaling alterations, previous studies have shown that intrapulmonary arteries exposure to engineered NPs alters vascular reactivity (Courtois et al. 2010; Ying et al. 2013). Calcium homeostasis is controlled by calcium intracellular stores (i.e. endoplasmic reticulum and mitochondria), and calcium influx through membrane channels, such as stretch-activated channels (SAC) (Filippini, D'Amore, and D'Alessio 2019). Therefore, alterations of calcium intracellular stores and/or SAC activity may lead to increased cytoplasmic calcium concentrations. SAC include the mechanosensitive ion channels TRPV (Transient Receptor Potential Vanilloid). TRPV1 and TRPV4 expression are increased in vascular cells, and these channels play a role in pulmonary vessels remodeling, a major PH pathophysiological feature (Ducret et al. 2010; Parpaite et al. 2016). In addition, Goswami et al. have suggested that TRPV4 channels are a potential target for NiONPs and participate in cellular homeostasis alteration by regulating microtubules and actin (Goswami et al. 2010). Interestingly, it has been shown that a 4 h-exposure to NiONPs ( $1\text{--}10\ \mu\text{g/mL}$ ) increases intracellular calcium concentration in BEAS-2B pulmonary epithelial cells, through an interaction between NiONPs and calcium channels such as TRPV4 (DI Bucchianico et al. 2018).

However, although endothelial dysfunction is known to play a major role in the pathogenesis of vascular diseases such as PH, the underlying cellular and molecular mechanisms by which NiONPs alter calcium signaling in human pulmonary endothelial

cells have not been reported yet. In this respect, the objectives of the proposed *in vitro* study are to assess these NiONPs-dependent mechanisms in human pulmonary artery endothelial cells (HPAEC). In this work, we first focused on characterizing the NiONPs used. Then, we investigated NiONPs-induced HPAEC cytotoxicity, oxidative stress, pro-inflammatory response, mitochondrial dysfunction, and apoptosis, as well as altered calcium signaling and nitric oxide (NO) bioavailability in these cells.

## Materials and methods

### Human pulmonary arterial endothelial cells culture

Human pulmonary arterial endothelial cells (HPAEC) were isolated from the pulmonary artery main branch of 2 donors, a 56-year-old Caucasian male and a 37-year-old Caucasian female (N°433Z034.1 and N°451Z031.14, respectively; PromoCell®, Germany). HPAEC were cultured in Endothelial Cell Growth Medium (ECGM) supplemented with Supplement Mix, following manufacturer's guidelines (PromoCell®). Cells were seeded at 20 000 cells/cm<sup>2</sup> on 25 cm<sup>2</sup> culture flasks and were maintained at 37 °C, in a 95% humidity air and 5% CO<sub>2</sub>. Cell passages were performed after about 80% confluence had been achieved. All experiments have been conducted on HPAEC from passages 2–8.

### Reagents and chemicals

HPAEC cells were cultured in ECGM from PromoCell®. The standard physiological salt solution (PSS) was composed of: 130 mM NaCl, 5.6 mM KCl, 8 mM HEPES, 11 mM Glucose, 1 mM Mg<sup>2+</sup> and 2 mM Ca<sup>2+</sup>; adjusted at pH = 7.4. The Krebs-HEPES Buffer (KHB) was composed of 118.4 mM NaCl, 4.7 mM KCl, 1.2 mM MgSO<sub>4</sub>, 4 mM NaHCO<sub>3</sub>, 1.2 mM KH<sub>2</sub>PO<sub>4</sub>, 2 mM CaCl<sub>2</sub>, 10 mM HEPES and 6 mM D-Glucose. Fluo-4-AM green dye (1 µM), MitoSOX<sup>TM</sup> red dye (5 µM), Fluo-4FF green dye (10 µM), TMRM red dye (100 nM), 4-Amino-5-Methylamino-2',7'-Difluorofluorescein Diacetate (DAF-FM) green dye (5 µM) and Hoechst 33342 blue dye (2 µM) were purchased from ThermoFischer Scientific, Invitrogen<sup>TM</sup> (France), except Rhod-2, AM red dye (1 µM) which was purchased from Euromedex (France). All of the following chemical reagents

were purchased from Sigma-Aldrich (France) and used as follows: ethylene glycol-bis(β-aminoethyl ether)-N,N,N',N'-tetraacetic acid (EGTA), as a chelator of extracellular calcium and diluted in ECGM (final concentration 5 mM); superoxide dismutase–polyethylene glycol (PEG-SOD) and catalase–polyethylene glycol (PEG-CAT), as antioxidant enzymes and diluted in ECGM (300 U/mL and 600 U/mL, respectively); GSK-1016790A, as a TRPV4 channel agonist (100 nM); 2-methyl-1-(3-morpholin-4-ylpropyl)-5-phenyl-N-[3-(trifluoromethyl)phenyl] pyrrole-3-carboxamide (HC-067047), as a TRPV4 channel antagonist (1 µM).

### NiO nanoparticles

#### NiONPs characterization

Nickel (II) oxide nanoparticles (NiONPs) (Cat. No.637130) were purchased from Sigma-Aldrich (USA). These particles partly characterized by the manufacturer have the following physical and chemical characteristics: mean aerodynamic diameter: 50 nm (as assessed by Transmission Electron Microscopy, TEM), density: 6.67 g/ml, purity: 99.8% trace metals basis, refractive index: 1.331 and viscosity: 0.888 cP. NiONPs were suspended in ECGM at a final concentration of 2 mg/ml and stored at 4 °C until use. Before use, stock suspensions were vortexed, sonicated 30 s three times (Vibracell 75186, 130 W, 56–60 Hz), and diluted extemporaneously in ECGM at appropriate concentrations (0.5–150 µg/cm<sup>2</sup>).

#### Hydrodynamic size distributions and zeta potential

The hydrodynamic size distribution of NiONPs dispersed in ECGM was assessed at a concentration of 9.5 µg/mL (5 µg/cm<sup>2</sup>) by Dynamic Light Scattering (DLS), using a VASCO particle size analyzer from Cordouan Technologies® (Pessac, France), as previously described (Deweirdt et al. 2020). The size distribution data were analyzed using a probabilistic self-learning algorithm, so-called Sparse Bayesian Learning (SBL), adapted for highly polydispersed particle suspensions, to improve the resolution of multimodal size distributions. To evaluate NiONPs surface charge, Zeta potential values of NiONPs were measured using laser Doppler electrophoresis and a Wallis zeta potential analyzer from Cordouan Technologies®. NiONPs were dispersed at 0.2 g/L in

1 mM  $\text{KNO}_3$ . The pH value of the dispersion was adjusted by adding droplets of 10%  $\text{HNO}_3$  or 1 M NaOH solutions. Six measurements were performed for each pH value. Then, in order to check the influence of serum proteins and of other components of the cell growth medium which can be adsorbed on their surface, NiONPs were incubated for 5 min (0.2 mg/ml), then the ECGM was centrifuged and dispersed in 1 mM HEPES adjusted to pH 7.4.

To investigate for all further experiments the mechanism of NiONPs-induced toxic effect in HPAEC, two-time points were performed (4 h or/and 24 h) according to kinetic preliminary studies.

### **NiONPs internalization**

Transmission Electronic Microscope (TEM) was used to study NiONPs internalization. Cells were seeded at 20 000 cells/cm<sup>2</sup> in Lab-Teck chambers (Dutsher, France), and cultured in supplemented ECGM, for 24 h at 37 °C and 5% CO<sub>2</sub>. Cells were then exposed or not to NiONPs at 5 µg/cm<sup>2</sup>. After a 4 h-exposure to NiONPs, cells were fixed with 1.6% paraformaldehyde and 2% glutaraldehyde in 0.08 M cacodylate buffer (pH 7.4) for 2 h at room temperature (RT). After washing in 0.1 M cacodylate buffer, cells were post-fixed in a mix of 1% osmium tetroxide (v/v)/1% potassium ferricyanide  $\text{K}_3\text{Fe}(\text{CN})_6$  (p/v) in 0.1 M cacodylate buffer, for 2 h, on ice in the dark. Then, samples were washed in water and stained in 0.5% aqueous uranyl acetate solution for 30 min at RT and in the dark. Subsequently, cells were washed, dehydrated through a series of graded ethanol, and finally embedded, first in a mixture of pure ethanol and epoxy resin 50/50 (v/v) (Epon 812; Delta Microscopie, Toulouse, France) for 2 h and then in 100% resin overnight at RT. The resin polymerization was achieved after 48 h at 60 °C. Samples were then cut using a diamond knife (Diatome, BielBienne, Switzerland) using an ultramicrotome (EM UCT, Leica Microsystems, Vienna, Austria). Ultrathin sections (65 nm) were laid on copper grids and then stained with Uranylless (Delta Microscopies, Toulouse, France) and lead citrate. Grids were examined with a Transmission Electron Microscope (H7650, Hitachi, Tokyo, Japan) at 80 kV.

### **Cytotoxic assay**

Cell viability was assessed by the determination of cell mitochondrial metabolic activity using the WST-1 (Water Soluble Tetrazolium) cell proliferation reagent (Roche, France) according to the manufacturer's recommendations. It is a colorimetric method for determining mitochondrial metabolic activity (viable cells). This assay, in which a succinate-tetrazolium reductase enzyme can convert a tetrazolium salt compound (WST-1) into an aqueous soluble and colored formazan, assumes that the relative number of viable cells is proportional to the mitochondrial enzymatic activity. Cells were seeded at 20 000 cells/cm<sup>2</sup> in a 96-well plate and cultured for 24 h. After a 24 h-exposition with NiONPs (1–150 µg/cm<sup>2</sup>), cells were rinsed with ECGM and incubated for 3 h with WST-1 reagent. The absorbance was measured at 450 nm by spectrophotometry using a microplate spectrophotometer reader (SPECTROstarNano2.10, BMG Labtech®, Germany). The working concentrations for all further experiments (for which the mortality rate was less than 30%) were all determined with this test.

### **Oxidative stress**

Cells were seeded at 20 000 cells/cm<sup>2</sup> in 12-well, 24-well, or 96-well plates and cultured for 24 h at 37 °C and 5% CO<sub>2</sub>. Cells were then exposed to NiONPs (0.25–5 µg/cm<sup>2</sup>) for 4 or 24 h.

### **Global reactive oxygen species production**

Intracellular ROS production was assessed using the CM-H<sub>2</sub>DCFDA probe (Fisher Scientific®), according to the manufacturer's recommendations and adapted from previous studies (Chen et al. 2010). The non-fluorescent CM-H<sub>2</sub>DCFDA reagent diffuses rapidly through the cell membrane and is hydrolyzed by intracellular esterases to a non-fluorescent oxidative sensitive form (CM-H<sub>2</sub>DCF) that is oxidized by ROS to generate a highly fluorescent adduct with a fluorescent intensity proportional to intracellular ROS production. Cells were rinsed with ECGM without serum and were pre-incubated for 20 min with CM-H<sub>2</sub>DCFDA probe (final concentration 20 µM) before a 4 h-exposure to NiONPs. Fluorescence intensity was measured by spectrofluorimetry at 485/520 nm (excitation/emission) by



using the FLUOstar Omega 2.10 plate reader, and the analyses were performed with the MARS Data Analysis Software 2.30 R3 (BMG Labtech®). Hydrogen peroxide, H<sub>2</sub>O<sub>2</sub>, was used as the positive control (1 mM).

#### **Cytoplasmic superoxide anion production**

Superoxide anion production was measured using the spin probe 1-hydroxy-3-methoxycarbonyl-2,2,5,5-tetramethylpyrrolidine (CMH, Noxygen®) according to the manufacturer's recommendations and as previously described (Deweirdt et al. 2017). EPR spin trapping is one of the specific techniques used to study free radical production such as the superoxide anion. However, the very short life span and the relatively low concentration of superoxide anion (O<sub>2</sub><sup>•-</sup>) made the measurement difficult to develop. The CMH probe has the property of being soluble and makes it possible to measure intracellular O<sub>2</sub><sup>•-</sup> (Dikalov et al. 2011; Konczol et al. 2012). Moreover, the CMH probe can be oxidized by O<sub>2</sub><sup>•-</sup> to generate a stable nitroxide radical (CMH<sup>•</sup>) easily detectable by EPR spectroscopy. After a 4 h-exposure to NiONPs, cells were incubated for 20 min with the spin-probe mix containing CMH (500 µM), diethyldithiocarbamate (5 µM), and deferoxamine (25 µM) in KHB solution. Then, HPAEC were scraped, homogenized, and frozen in a syringe in liquid nitrogen before EPR analysis. All the EPR spectra were recorded using the Spectrometer X Miniscope MS200 (Magnettech®, Germany). The EPR parameters have been previously described (Deweirdt et al. 2017). Following EPR spectra readings, protein quantities were measured by a Lowry test (Lowry reagent, Sigma Aldrich®), according to the manufacturer's recommendations. The results were normalized to protein quantities and expressed as EPR signal amplitudes in arbitrary units (AU)/mg of protein.

#### **Mitochondrial O<sub>2</sub><sup>•-</sup> production**

Production of mitochondrial superoxide anion (O<sub>2</sub><sup>•-</sup><sub>mt</sub>) was assessed using MitoSOX™ red dye (ThermoFischer®), according to the manufacturer's recommendations by confocal microscopy (TE 2000, Nikon). After a 4 h-exposure to NiONPs, cells were incubated for 30 min (37 °C, in the dark), with a MitoSOX probe in physiological salt solution (PSS). The MitoSOX probe was co-incubated with a

mitochondrial probe (Mitotracker) and a nucleus probe (Hoechst 33342). Fluorescence intensity was measured for MitoSOX at 543/605 nm, Mitotracker at 488/515 nm, and Hoechst 33342 at 408/450 nm (excitation/emission). For all the confocal microscopy experiments, the plates were observed with an X 200 magnification with an oil immersion objective on a laser scanning confocal microscope. MitoSOX fluorescence intensity is proportional to the rate of probe oxidation. Analyses were performed using the NIS-Elements AR software 3.0 and Microsoft Office Excel.

#### **Superoxide dismutase enzyme activity**

The superoxide dismutase (SOD) enzymatic activity was measured with a commercially available kit (19160 SOD determination kit, Sigma-Aldrich®, USA). This kit also uses WST-1, which produces a water-soluble formazan dye upon reduction with the superoxide anion. The rate of the reduction with O<sub>2</sub><sup>•-</sup> is linearly related to the xanthine oxidase activity and is inhibited by SOD. The IC<sub>50</sub> (50% inhibition of SOD activity) was determined by a colorimetric method. Inhibition of SOD activity can be quantified by measuring the decrease in color development at 440 nm. After a 24 h-exposure to NiONPs, supernatants, and cells were used for analysis according to the manufacturer's recommendations, to determine both intracellular and extracellular SOD activity. The absorbance of supernatants and cells was measured at 440 nm by spectrophotometry using a microplate spectrophotometer reader (SPECTROstarNano2.10, BMG Labtech®, Germany).

#### **Production of nitric oxide (NO) and NO metabolites**

Cells were seeded at 20 000 cells/cm<sup>2</sup> in 12-well or 96-well plates and cultured for 24 h at 37 °C and 5% CO<sub>2</sub>. Cells were then exposed to NiONPs (0.5–5 µg/cm<sup>2</sup>) for 4 or 24 h.

#### **Production of NO**

Production of NO was assessed by confocal microscopy using the DAF-FM probe (ThermoFischer®), according to the manufacturer's recommendations. After a 4 h or 24 h exposure with NiONPs, cells were incubated for 30 min (37 °C, in the dark), with a

DAF-FM probe in PSS, and co-incubated with a nucleus probe (Hoechst 33342). Fluorescence intensities were measured at 488/515 nm (excitation/emission) for the DAF-FM and at 408/450 nm for the Hoechst 33342. The DAF-FM fluorescence intensity is proportional to the rate of probe oxidation. The analyses were performed using the NIS-Elements AR software 3.0 and Microsoft Office Excel.

#### ***Production of NO metabolites***

Nitrite and nitrate products were assessed in HPAEC supernatants by using the Griess reagent (Sigma-Aldrich®), according to the manufacturer's recommendations. After a 24 h-exposure to NiONPs, the supernatants were removed, collected, and centrifuged at 10 000 g for 10 min at 4 °C. The supernatants were then analyzed according to the manufacturer's guidelines and the absorbance was measured at 540 nm by spectrophotometry, using a microplate spectrophotometer reader (SPECTROstarNano2.10, BMG Labtech®, Germany). *N*<sub>ω</sub>-Nitro-L-arginine methyl ester hydrochloride (L-Name) was used as a negative control (final concentration 10<sup>-4</sup> M) and Sodium nitroprusside (SNP) was used as a positive control (final concentration 10<sup>-4</sup> M).

#### ***Endothelin-1 production***

Cells were seeded at 20 000 cells/cm<sup>2</sup> in a 12-well plate and cultured for 24 h, at 37 °C and 5% CO<sub>2</sub>. Cells were rinsed with the culture medium and exposed to NiONPs (0.5–5 µg/cm<sup>2</sup>) for 24 h. Supernatants were then collected, centrifuged at 10 000 g for 10 min at 4 °C, and analyzed using Endothelin-1 kit (Endothelin-1 ELISA kit, Enzo Life Sciences®, France), according to the manufacturer's guidelines. The absorbance was measured at 450 nm by spectrophotometry using a microplate spectrophotometer reader (SPECTROstarNano 2.10, BMG Labtech®, Germany).

#### ***Pro-inflammatory effects: expression and secretion of interleukin (IL)-6***

Cells were seeded at 20 000 cells/cm<sup>2</sup> in a 12-well plate and cultured for 24 h, at 37 °C and 5% CO<sub>2</sub>. Cells were rinsed with the culture medium and

exposed to NiONPs (0.5–5 µg/cm<sup>2</sup>) for 24 h. Supernatants were then collected, centrifuged at 10 000 g for 10 min at 4 °C, and analyzed using an ELISA kit (Human IL-6 DuoSet® ELISA R&D Systems, USA), according to the manufacturer's guidelines. The absorbance was measured at 450 nm and corrected at 570 nm by spectrophotometry using a microplate spectrophotometer reader (SPECTROstarNano 2.10, BMG Labtech®, Germany).

#### ***Cytoplasmic, endoplasmic reticulum, and mitochondrial calcium measurements***

Variations in intracellular calcium [Ca<sup>2+</sup>]<sub>i</sub>, endoplasmic reticulum (ER) calcium [Ca<sup>2+</sup>]<sub>ER</sub> and mitochondrial calcium [Ca<sup>2+</sup>]<sub>m</sub> were detected respectively using the Fluo-4-AM green dye, the Fluo-4FF AM green dye and the Rhod-2 AM red dye, according to the manufacturer's guidelines. Cells were seeded at 20 000 cells/cm<sup>2</sup> in a 96-well plate and cultured for 24 h at 37 °C and 5% CO<sub>2</sub>. After a 4 h-exposure with NiONPs (0.5–5 µg/cm<sup>2</sup>), cells were incubated for 30 min (37 °C, in the dark), with the different fluorescent probes in PSS. Some cells were pretreated for 1 h with HC-067047 (1 µM) (which was then also left during exposure to NiONPs). Some cells were also incubated with EGTA (5 mM) during the experiments. An increase in [Ca<sup>2+</sup>]<sub>i</sub> after cell treatment with the TRPV4 agonist GSK-1016790A (10 nM) was also evaluated. The Fluo-4-AM probe, Rhod-2, AM probe, and Fluo-4FF, AM probe were co-incubated with a nucleus probe (Hoechst 33342). The plates were observed at X 200 magnification with an oil immersion objective on a laser scanning confocal microscope (TE 2000, Nikon). The fluorescence intensity was measured for Rhod-2 at 543/605 nm, for Fluo-4-AM and Fluo-4FF at 488/515 nm and for Hoechst 33342 at 408/450 nm (excitation/emission). For each experiment 20 to 30 cells were analyzed per well. The analyses were performed using NIS-Elements AR software 3.0 and Microsoft Office Excel.

#### ***Mitochondrial activity***

##### ***Mitochondrial membrane potential measurement***

The mitochondrial membrane potential (ΨMP) was measured by confocal microscopy using TMRM red dye (Tetramethylrhodamine, Methyl Ester,

Perchlorate, ThermoFischer) according to the manufacturer's guidelines. Cells were seeded at 20 000 cells/cm<sup>2</sup> in a 96-well plate and cultured for 24 h at 37 °C and 5% CO<sub>2</sub>. After a 4 h-exposure to NiONPs (0.5–5 µg/cm<sup>2</sup>), cells were incubated for 20 min (37 °C, in the dark) with a TMRM fluorescent probe in PSS. The TMRM probe was co-incubated with a nucleus probe (Hoechst 33342). The fluorescence intensity was then measured at 543/605 nm (excitation/emission). The analyses were performed using the NIS-Elements AR software 3.0 and Microsoft Office Excel.

### Mitochondrial mass

The mitochondrial mass was measured using confocal microscopy using the Mitotracker green dye (ThermoFischer) according to the manufacturer's guidelines. Cells were seeded at 20 000 cells/cm<sup>2</sup> in a 96-well plate and cultured for 24 h at 37 °C and 5% CO<sub>2</sub>. After a 4 h-exposure to NiONPs (0.5–5 µg/cm<sup>2</sup>),

Canto flow cytometer (Bioscience®, France) to detect life, apoptotic, and necrotic cells.

### Gene expression

A polymerase chain reaction (PCR) was performed to evaluate IL-6, TRPV4, and bcl-2 mRNA expressions. Cells were seeded at 20 000 cells/cm<sup>2</sup> in a 12-well plate and cultured for 24 h at 37 °C and 5% CO<sub>2</sub>. Cells were rinsed with the culture medium and exposed to NiONPs (0.5–5 µg/cm<sup>2</sup>) for 24 h. After a 24 h-exposure, mRNA extraction and purification were performed using a commercially available kit (SV Total RNA Isolation System, Promega), according to the manufacturer's recommendations. Reverse transcription was carried out by M-MLV (Moloney Murine Leukemia Virus) Reverse Transcriptase kit (Promega). Finally, a real-time quantitative PCR (qPCR) analysis was performed using a LightCycler® 480 (Roche) with a first cycle at 95 °C for 2 min, fol-

Primers	Sense	Antisense
IL-6	5'-ACAGCCACTCACCTCTTCAG-3'	5'-TGGAAGCATCCATCTTTTC-3'
TRPV4	5'-CGCAAGTGGAGGACTGATGA-3'	5'-TAGAAATGAGTGGGCAGAGAAGCT-3'
Bcl-2	5'-GGCCTTCTTTGAGTTCGGTG-3'	5'-CATCCCAGCCTCCGTTATCCTG-3'
RPL13	5'-GGGAGCAAGGAAAGGGTCTTA-3'	5'-CACCTGCAAAATCTCCGAGT-3'
GAPDH	5'-CACATGGCCTCCAAGGAGTAA-3'	5'-TGAGGGTCTCTCTTCTCTTGT-3'
Gusb	5'-TGAAATCGGCAAAATTCAAAT-3'	5'-CCATCTGGGTCTGGATCAAAA-3'

cm<sup>2</sup>), cells were incubated for 30 min (37 °C, in the dark) with the MitoTracker probe in PSS. The Carbonylcyanure m-chlorophénylhydrazone (cccp) was used as a positive control (final concentration 5 µm). The MitoTracker probe was co-incubated with a nucleus probe (Hoechst 33342). The fluorescence intensity was measured at 408/450 nm (excitation/emission). The analyses were performed using the NIS-Elements AR software 3.0 and Microsoft Office Excel.

### Apoptosis induction

The Annexin V-FITC/propidium iodide (PI) kit (ThermoFischer) was used according to the manufacturer's guidelines for the detection of apoptosis and necrosis. Cells were seeded at 20 000 cells/cm<sup>2</sup> in a 12-well plate and cultured for 24 h at 37 °C and 5% CO<sub>2</sub>. After a 24 h-exposure to NiONPs (0.5–10 µg/cm<sup>2</sup>), supernatants and cells were analyzed for 1 h by flow cytometry using a BD FACS

lowed by 45 cycles at 95 °C for 15 s and at 60 °C for 1 min. The ribosomal protein (RPL13), the glyceraldehyde-3-phosphate dehydrogenase (GAPDH), and the β-glucuronidase (Gusb) genes were used as internal controls. The following primer sequences were used:

### Statistical analysis

Each experimental condition was independently repeated several times (n indicates the number of experiments) and for each independent experiment, 3–8 wells per condition were assessed. Data are expressed as mean ± Standard Error of the Mean (SEM) for n independent experiments. Statistical analyses have been performed using either one-way ANOVA followed by Tukey's post-test for multiple comparisons when  $n > 30$ , or Kruskal–Wallis test followed by Dunn's post-test when  $n < 30$ . (\* $p < 0.05$ , \*\* $p < 0.01$ , \*\*\* $p < 0.001$  and \*\*\*\* $p < 0.0001$ ) All data were analyzed using Graphpad PRISM software



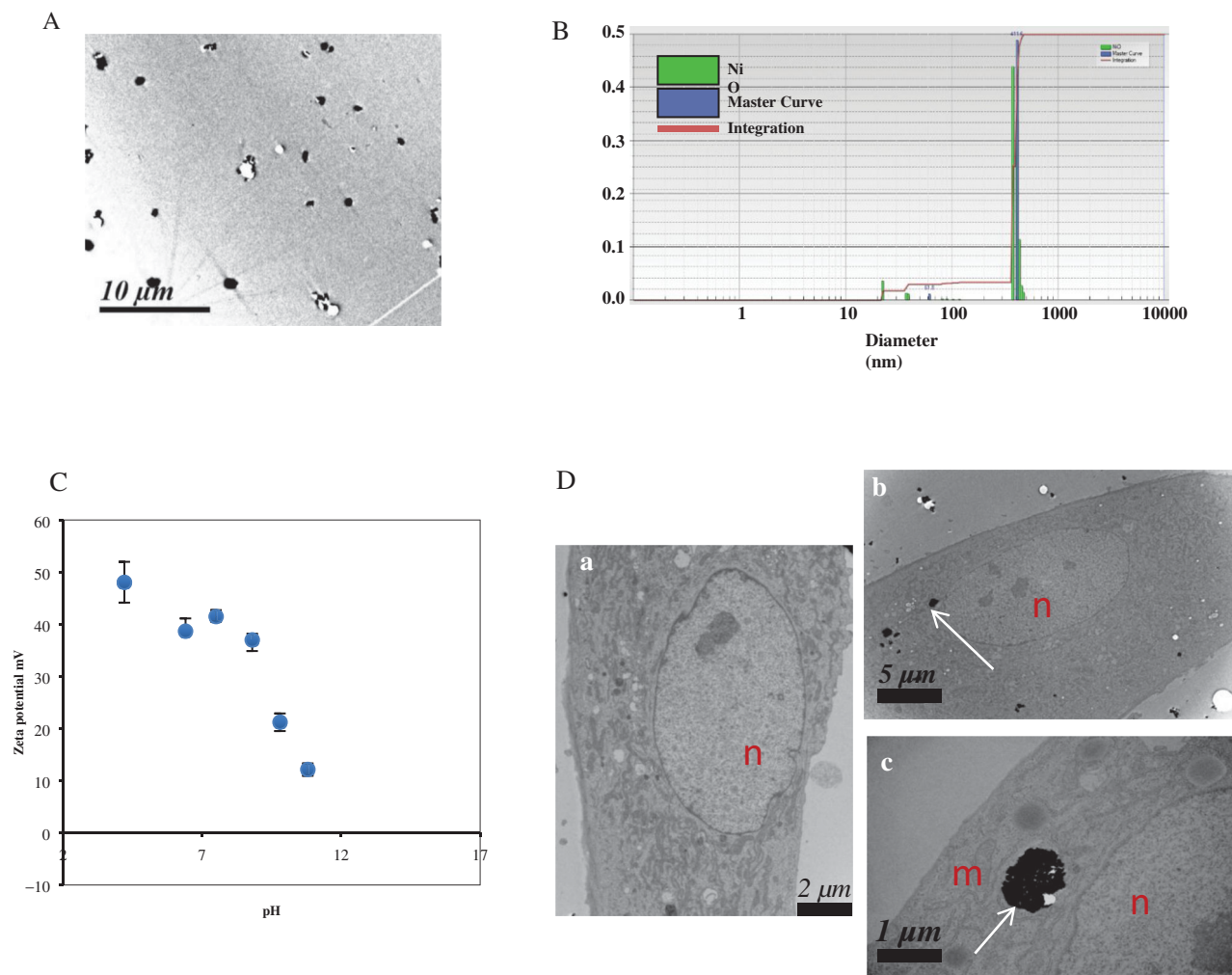


**Figure 1.** Characteristics of NiONPs in ECGM. (A) NiONPs in ECGM observed by transmission electronic microscope (TEM). (B) Size distribution of NiONPs ( $5 \mu\text{g}/\text{cm}^2$ ) measured by DLS. (C) Zeta potential of NiONPs (Da) HPAEC observed by TEM, control (X12000). (Db) NiONPs ( $5 \mu\text{g}/\text{cm}^2$ ) internalization and intracellular localization in HPAEC (X15000). White arrows show intracellular NiONPs aggregate, 'n' corresponds to the nucleus, 'm' corresponds to the mitochondria. Statistically significant at  $p < 0.05$ (\*),  $p < 0.01$ (\*\*) and  $p < 0.001$ (\*\*\*) as compared to untreated control cells.

(v6, Graphpad Software).  $p$ -Values  $< 0.05$  were considered significant.

## Results

### Characterization of NiONPs

Dynamic light scattering measurement (DLS) was implemented to assess the colloidal stability state of NiONPs in the culture medium. The results at  $5 \mu\text{g}/\text{cm}^2$  showed a peak detected around  $400 \pm 20 \text{ nm}$ , indicating a flocculation state of NiONPs of  $50 \text{ nm}$  unit size (Figure 1(A,B)). In Figure 1(C), we observe that NiONPs display positive zeta potential values from pH 4 to 11 with a decrease in alkaline media. These results are in accordance with

the literature showing zero point of charge around pH 11 (Zheng et al. 2017). For the physiological pH value (i.e. 7.4) NiONPs are positively charged with a quite high potential value of around  $+40 \text{ mV}$ . The value of the zeta potential after incubation in ECGM is radically modified, becomes negative ( $-26.26$ ). Serum proteins present in the culture medium are mostly negatively charged with  $\text{pI} < 7.4$ . This change of zeta potential after incubation may be due to a protein corona formation, mainly driven by electrostatic interaction at NiONPs surface (among other types of interactions that may occur). After a second washing with  $1 \text{ mM}$  HEPES buffer at pH 7.4, the absolute potential value slightly increased further ( $-36.69$ ), which may be explained by a screening of counter ions that are displaced

during the second washing. This result also suggests that some of these proteins are strongly adsorbed on NiONPs.

### ***Internalization of NiONPs in HPAEC***

TEM was performed to observe NiONPs uptake and localization in HPAEC after a 4 h-exposure ( $5 \mu\text{g}/\text{cm}^2$ ). Control cells are shown in Figure 1(Da). After a rapid internalization, NiONPs were mainly clustered in vesicles in the cytoplasm (Figure 1(Db)). Internalized NiONPs were mostly organized in aggregates of various sizes. NiONPs were also localized near the nucleus or near mitochondria (Figure 1(Dc)).

### ***NiONPs decrease cell viability***

To understand the mechanism of NiONPs-induced effect in HPAEC, the nontoxic range of NiONPs concentration (mortality rate  $< 30\%$ ) was first investigated by using the WST-1 test. Cytotoxic effect was evaluated on HPAEC after a 24 h-treatment with NiONPs. The results showed a significant and concentration-dependent decrease of cell viability starting from  $2 \mu\text{g}/\text{cm}^2$  (78.25% of viability,  $*p < 0.05$ ) as compared to untreated cells (Figure 2(A)). These results also showed that HPAEC mitochondrial activity decreased in a concentration-dependent manner upon exposure to NiONPs.

### ***NiONPs induce oxidative stress***

To investigate the oxidative stress, different assays were performed, to measure global ROS production, cytoplasmic superoxide anion ( $\text{O}_2^-$ ) production, and mitochondrial  $\text{O}_2^-$  production. In addition, the antioxidant response has been evaluated by measuring SOD enzymatic activity.

### ***Cytoplasmic ROS production***

After a 4 h-exposure of HPAEC to NiONPs ( $0.25$ – $5 \mu\text{g}/\text{cm}^2$ ), we observed a significant and concentration-dependent increase in intracellular global ROS production (13.28%; 14.08%; 14.04% and 15.57% respectively for 0.5, 2.5, 1, and  $5 \mu\text{g}/\text{cm}^2$ ) as compared to untreated cells (Figure 2(B)).

### ***Cytoplasmic $\text{O}_2^-$ production***

After a 4 h-exposure to NiONPs ( $0.5$ – $5 \mu\text{g}/\text{cm}^2$ ), we observed a significant and concentration-dependent increase in intracellular  $\text{O}_2^-$  production (5854.29 AU/(mg/ml) of protein and 5881.67 AU/(mg/ml) of proteins, respectively for 2.5 and  $5 \mu\text{g}/\text{cm}^2$ ) as compared to untreated cells (Figure 2(C)).

### ***Mitochondrial $\text{O}_2^-$ production***

After a 4 h-exposure of HPAEC to NiONPs ( $0.5$ – $5 \mu\text{g}/\text{cm}^2$ ), we observed a significant concentration-dependent increase in mitochondrial  $\text{O}_2^-$  production (143.36% and 170.17% respectively for 2.5 and  $5 \mu\text{g}/\text{cm}^2$ ), as compared to untreated cells (Figure 2(D)).

### ***SOD activity***

After a 24 h-exposure of HPAEC to NiONPs ( $0.5$ – $5 \mu\text{g}/\text{cm}^2$ ), a significant decrease in SOD enzymatic activity was observed at the two highest concentrations tested (2.5 and  $5 \mu\text{g}/\text{cm}^2$  with 58.13% and 59.56% respectively), compared to the untreated cells (Figure 2(E)).

### ***NiONPs increase IL-6 expression and secretion***

IL-6 mRNA expression and IL-6 secretion were measured in HPAEC by qPCR and ELISA assays, respectively. After a 24 h-exposure to NiONPs ( $0.5$ – $5 \mu\text{g}/\text{cm}^2$ ), the results showed a significant increase in both IL-6 mRNA expression and IL-6 secretion at  $5 \mu\text{g}/\text{cm}^2$  (80.30 pg/mg of proteins) as compared to untreated cells (Figure 3(A,B)). In order to determine whether the inflammatory response induced by NiONPs involved oxidative stress, the same experiments were performed using antioxidant enzymes. After a 1-h pretreatment of HPAEC with both PEG-SOD and PEG-CAT, followed by a 24 h-exposure to NiONPs ( $5 \mu\text{g}/\text{cm}^2$ ), no significant effect on IL-6 secretion was observed anymore, as compared to untreated cells (Figure 3(C)). These results, therefore, show that ROS production contributes to the pro-inflammatory response observed in HPAEC after exposure to NiONPs ( $5 \mu\text{g}/\text{cm}^2$ ).

### ***NiONPs increase the cytosolic calcium level***

The basal cytoplasmic calcium concentration was measured in HPAEC. After a 4 h and a 24 h-exposure

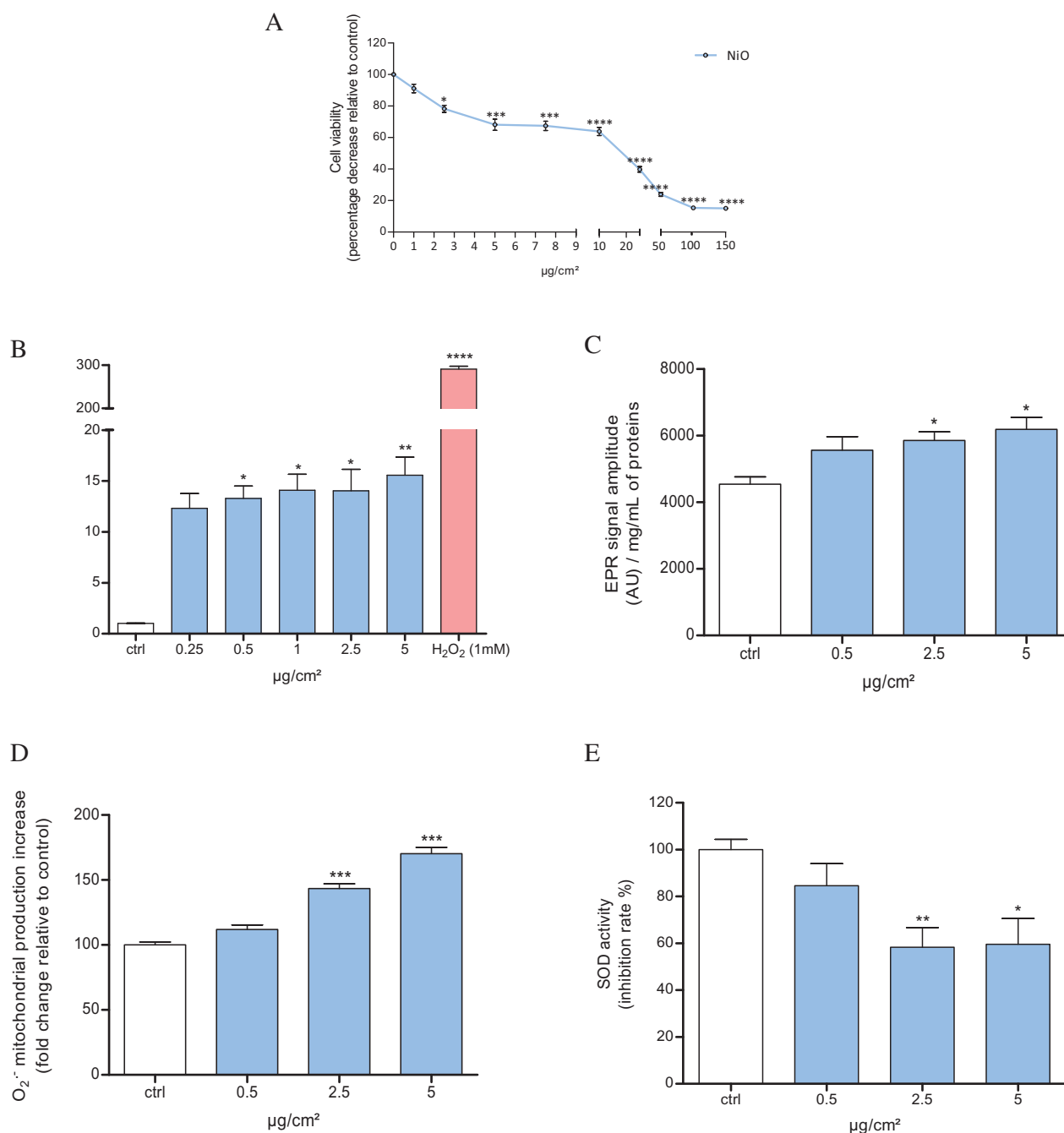


**Figure 2.** Viability cells and Oxidative stress on HPAEC after NiONPs exposure. (A) Cell viability was measured after a 24 h-exposure with NiONPs ( $1\text{--}150\text{ }\mu\text{g}/\text{cm}^2$ ) by the colorimetric WST-1 assay. Results are expressed as the percentage of cell viability in treated cells, as compared to control cells (100%). Data were mean  $\pm$  SEM of four independent experiments,  $n=4$  (eight wells/concentration). (B) Global intracellular ROS production after 4 h-exposure with NiONPs was measured by spectrofluorimetry via CM- $\text{H}_2\text{DCFDA}$  probe assay. (C) Intracellular  $\text{O}_2^-$  production after 4 h-exposure with NiONPs, measured by EPR spectrometer with CMH probe. Results are expressed in EPR signal amplitude in arbitrary units (AU)/mg/mL of proteins. (D) Mitochondrial  $\text{O}_2^-$  production after 4 h-exposure with NiONPs, measured with MitoSOX probe ( $5\text{ }\mu\text{M}$ ), by confocal microscopy. The values were normalized to untreated cells, and results are expressed as the fold change of MitoSOX probe fluorescence intensity, relative to control cells. (E) SOD activity was measured by a colorimetric test after 24 h-exposure with NiONPs ( $0.5\text{--}5\text{ }\mu\text{g}/\text{cm}^2$ ). The values were normalized to the untreated cells and results were expressed as the SOD activity inhibition rate relative to the control cells. Data were mean  $\pm$  SEM of three independent experiments,  $n=3$  (three wells/concentration). Statistically significant at  $p < 0.05$  (\*),  $p < 0.01$  (\*\*), and  $p < 0.001$  (\*\*\*), as compared to untreated control cells.

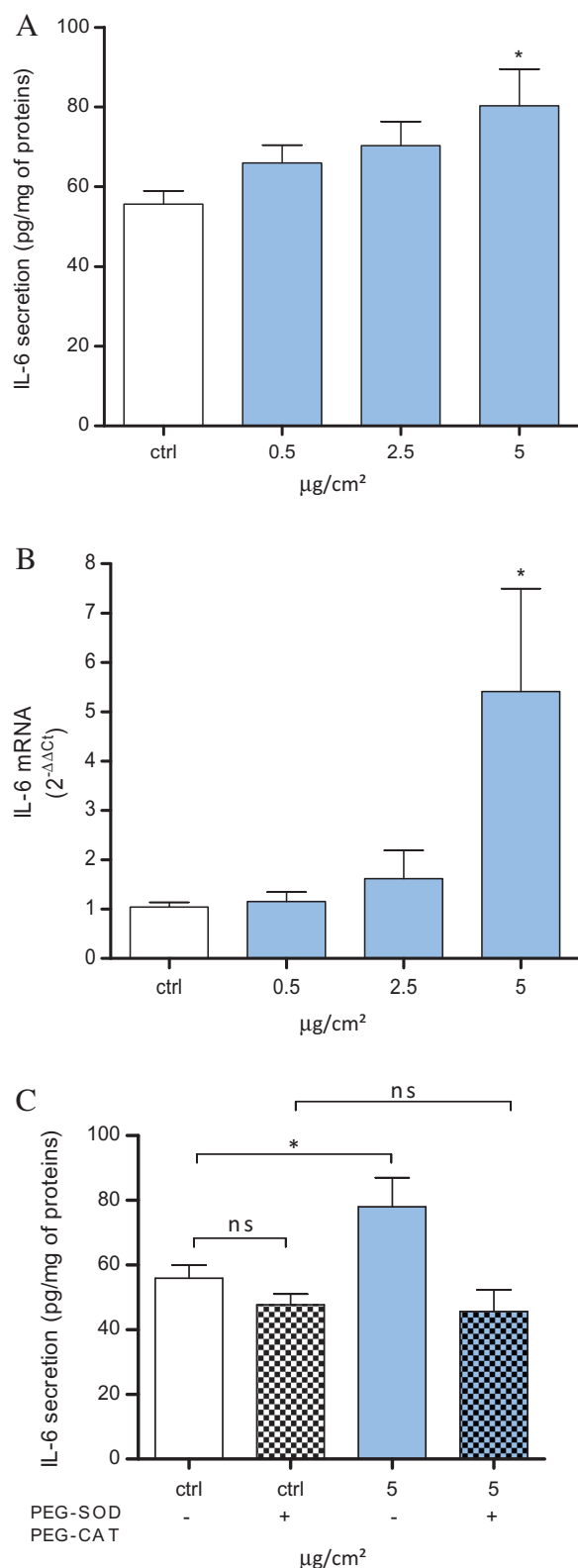


**Figure 3.** IL-6 secretion and expression in HPAEC after 24 h-exposure with NiONPs (0.5–5  $\mu\text{g}/\text{cm}^2$ ). (A) Secretion of IL-6 measured by ELISA assay. The results were expressed as pg/mg of proteins. Data were mean  $\pm$  SEM of six independent experiments,  $n = 6$  (three wells/concentration). (B) IL-6 mRNA expression measured by RT-qPCR. The results were expressed as the fold change of IL-6 mRNA expression relative to the

**Figure 3.** (Continued)

control cells. Data were mean  $\pm$  SEM of five independent experiments ( $n = 5$ ) (three wells/concentration). (C) Effect of antioxidant enzymes after or not 1 h-pretreatment with PEG-SOD (600 U/mL) and PEG-catalase (300 U/mL) measured by ELISA. Data were mean  $\pm$  SEM of three independent experiments ( $n = 3$ ) (three wells/concentration). Results were expressed as pg/mg of proteins in the supernatant. Statistically significant at  $p < 0.05$  (\*) as compared to untreated control cells.

to NiONPs (0.5–5  $\mu\text{g}/\text{cm}^2$ ) calcium imaging was assessed with Fluo-4-AM probe, and the results showed that in HPAEC, after a 4 h-exposure, a significant concentration-dependent increase of the basal cytoplasmic calcium levels was observed (121.17%, 128.1%, and 156.19%, respectively for 0.5, 2.5, and 5  $\mu\text{g}/\text{cm}^2$ ), as compared to untreated cells (Figure 4(A)). Interestingly, after a 24 h-exposure to NiONPs, this significant increase of cytoplasmic calcium levels was still observed (120.34% and 129.74% for 2.5 and 5  $\mu\text{g}/\text{cm}^2$ , respectively), as compared to untreated cells (Figure 4(B)), suggesting that this alteration of calcium homeostasis was maintained throughout the exposure duration for 2.5 and 5  $\mu\text{g}/\text{cm}^2$ .

### **Oxidative stress leads to increased cytoplasmic calcium levels**

In the second set of experiments, in order to determine whether the NiONPs-induced alterations in intracellular calcium levels were correlated to oxidative stress, the same experiments were performed using antioxidant enzymes. With a 1-h pretreatment with PEG-SOD and PEG-CAT, prior to a 4 h-exposure to NiONPs (0.5–5  $\mu\text{g}/\text{cm}^2$ ), a significant concentration-dependent increase in cytoplasmic calcium levels was still observed (110.04% and 114.68% for 2.5 and 5  $\mu\text{g}/\text{cm}^2$ , respectively) as compared to untreated cells (Figure 4(C)). However, pretreatment with antioxidant enzymes significantly inhibited the increase in cytoplasmic calcium levels for 0.5  $\mu\text{g}/\text{cm}^2$ , as compared to NiONPs-treated cells without antioxidant enzymes. Therefore, the results suggest that ROS production is only partially involved in the alterations of calcium levels. Thus, additional experiments were performed in order to elucidate another potential mechanism involved in NiONPs-induced calcium signaling alterations.

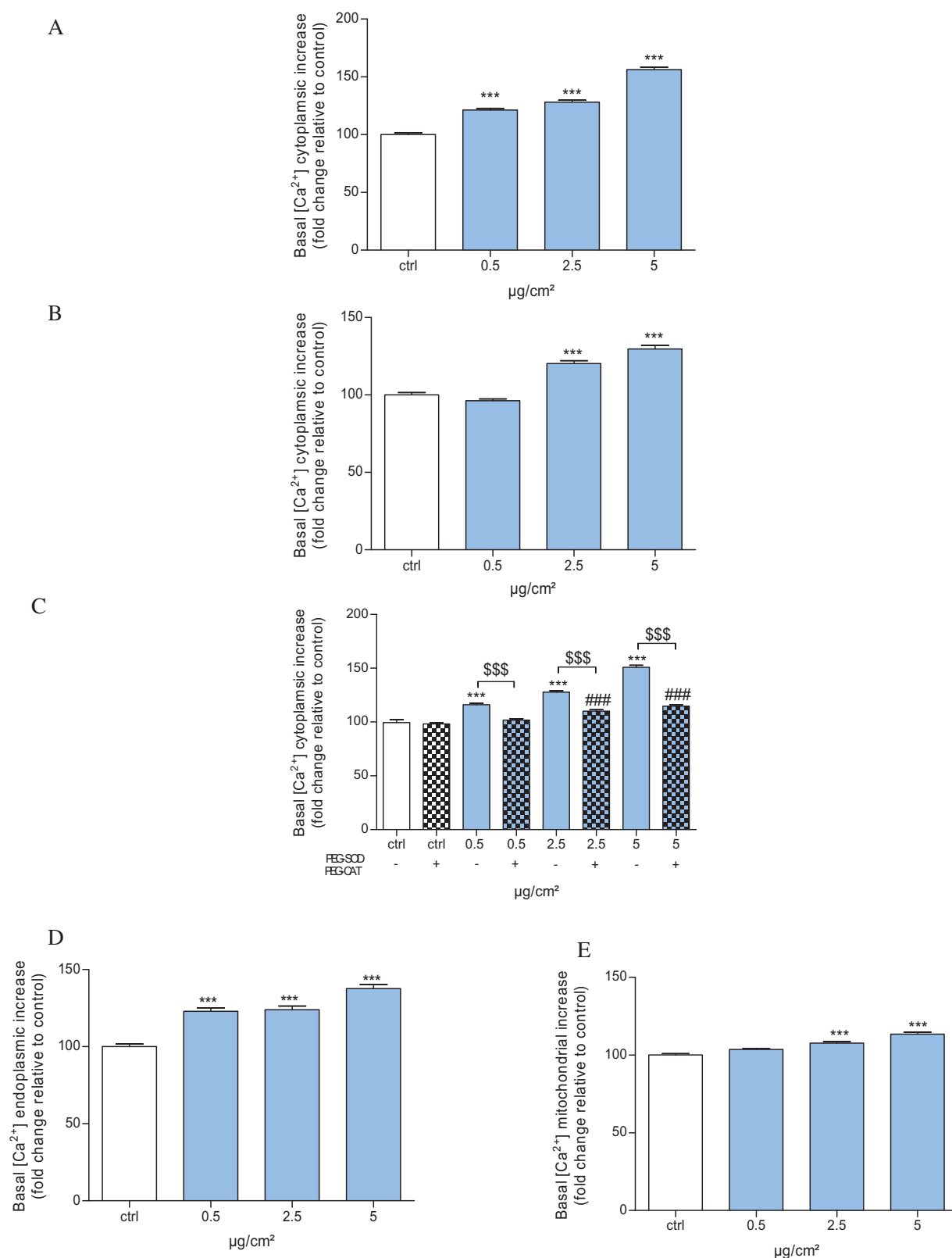


**Figure 4.** Calcium level in HPAEC with NiONPs (0.5–5 µg/cm²). Cytoplasmic ( $[Ca^{2+}]_i$ ), endoplasmic reticulum ( $[Ca^{2+}]_{ER}$ ) and mitochondrial calcium ( $[Ca^{2+}]_m$ ) levels was measured by confocal microscopy respectively with Fluo-4, AM probe (1 µM), Fluo-4FF, AM probe (10 µM) and Rhod-2AM probe (1 µM). (A)  $[Ca^{2+}]_i$  in cells after 4 h-exposure with NiONPs. (B)  $[Ca^{2+}]_i$  in cells after 24 h-exposure. (C) Effect of antioxidant enzymes after or not 1 h-pretreatment with PEG-SOD (600 U/mL) and PEG-catalase (300 U/mL) and 4 h-exposure with NiONPs. (D)  $[Ca^{2+}]_{ER}$  in cells after 4 h-exposure with NiONPs. (E)  $[Ca^{2+}]_m$  in cells after 4 h-exposure with NiONPs. All values were normalized to the untreated cells and results were expressed as the fold change of the probes fluorescence intensity relative to the control cells (100%). Data are mean ± SEM of three independent experiments ( $n = 3$ ), (six wells/concentration). Statistically significant at  $p < 0.001$ \*\*\*, as compared to untreated cells, statistically significant at  $p < 0.001$ \*\*\*, as compared to cells pretreated with antioxidant enzymes.



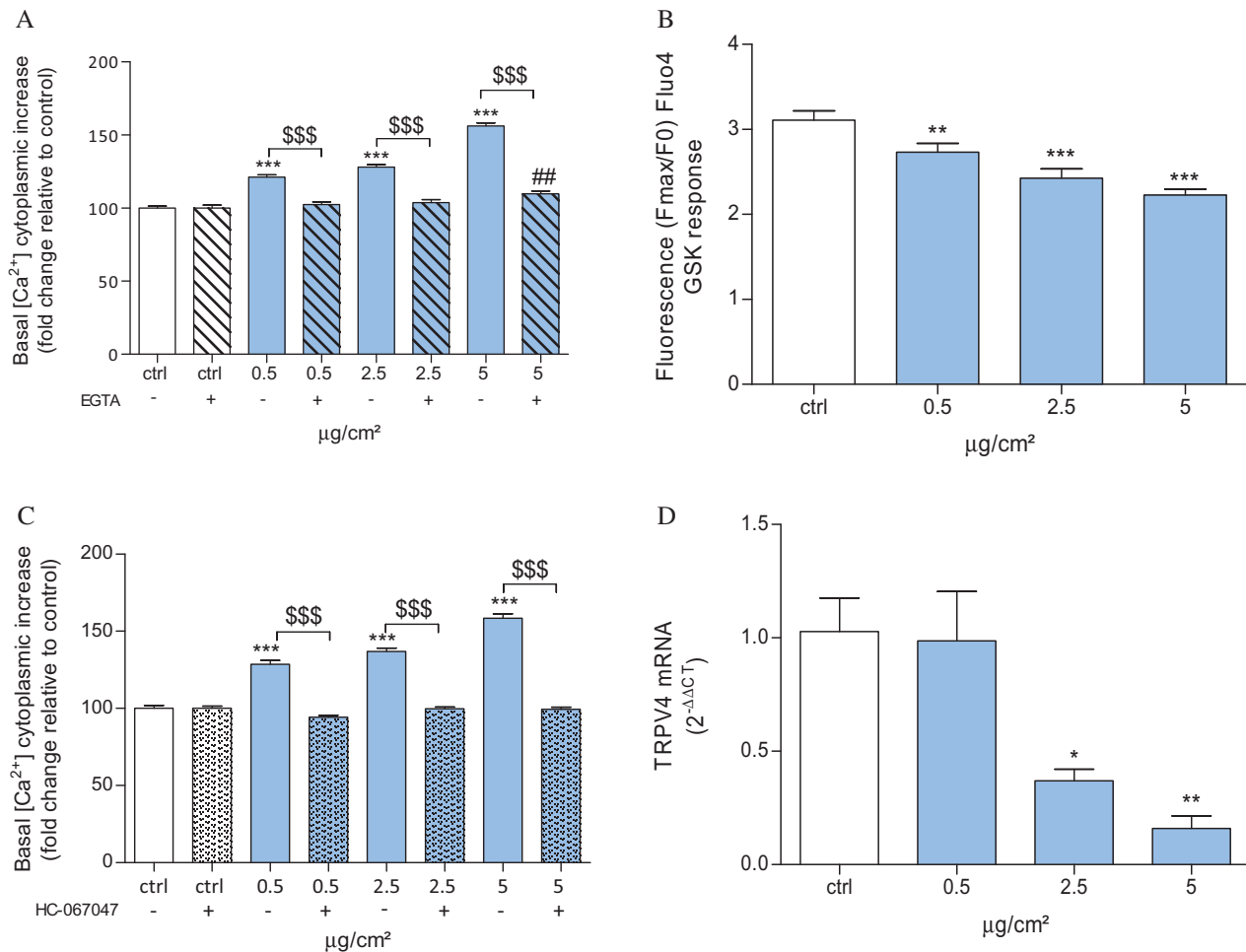


**Figure 5.** Effect of extracellular calcium and TRPV4 channel on [Ca<sup>2+</sup>]<sub>i</sub> level rise after NiONPs exposition (0.5–5 µg/cm<sup>2</sup>). [Ca<sup>2+</sup>]<sub>i</sub> was measured with Fluo-4, AM probe (1 µM), by confocal microscopy. (A) Effect of extracellular calcium on [Ca<sup>2+</sup>]<sub>i</sub> level rise after 4 h-exposure with NiONPs in the presence (1.6 mM [Ca<sup>2+</sup>]<sub>e</sub>) or in absence of extracellular calcium (0 mM [Ca<sup>2+</sup>]<sub>e</sub>). (B) Effect of TRPV4 agonist after 4 h-exposure with NiONPs: The GSK response (100 nM) was expressed as the Fluo-4 fluorescence ratio (F<sub>max</sub>/F<sub>0</sub>). (C) Effect of TRPV4 antagonist after 4 h-exposure with NiONPs and after or not 1 h-pretreatment with HC-067047 (1 µM). Data were mean ± SEM of three independent experiments, (n = 3) (five wells/concentration). (D) TRPV4 mRNA expression after 24 h-exposure with NiONPs, measured by RT-qPCR. The results were expressed as the fold change of TRPV4 mRNA expression relative to the control cells. Data were mean ± SEM of four independent experiments, (n = 4) (three wells/concentration). Statistically significant at *p* < 0.01 (\*\*) and *p* < 0.001 (\*\*\*) as compared to untreated cells statistically significant at *p* < 0.001(\$\$\$), as compared to both condition (HC pretreatment or not).

### NiONPs alter calcium channels

To assess the role of extracellular sources in cytoplasmic [Ca<sup>2+</sup>]<sub>i</sub> rise, HPAEC were exposed to NiONPs (0.5–5 µg/cm<sup>2</sup>) in the presence or in the absence of extracellular calcium, by use of the extracellular calcium chelator (EGTA). In the presence of EGTA, the result showed a significant increase in cytoplasmic calcium levels, but only at the highest concentration of 5 µg/cm<sup>2</sup> (109.71%) as compared to untreated cells (Figure 5(A)). This observation suggests that for lower concentrations, NiONPs-induced increase in cytoplasmic calcium levels only involves extracellular calcium, whereas at

the highest concentration, NiONPs-induced cytoplasmic [Ca<sup>2+</sup>]<sub>i</sub> rise may involve both extracellular and intracellular calcium stores. Then, the activity of the mechanoreceptor transient receptor potential vanilloid 4 (TRPV4) channels was assessed. TRPV4 involvement was studied by calcium imaging using a TRPV4 activator (GSK1016790A) and a TRPV4 antagonist (HC-067047). The results in HPAEC after a 4 h-exposure to NiONPs (0.5–5 µg/cm<sup>2</sup>) showed a significant concentration-dependent decrease in the GSK1016790A response by 0.5 µg/cm<sup>2</sup>, as compared to untreated cells (Figure 5(B)). By contrast, no significant effect of HC-067047 on NiONPs in basal

calcium cytoplasmic level was observed, as compared to control cells (Figure 5(C)). The analysis of TRPV4 mRNA expression after a 24 h-exposure to NiONPs showed a significant decreased TRPV4 expression ( $0.37 \cdot 2^{-\Delta\Delta C_t}$ ,  $0.16 \cdot 2^{-\Delta\Delta C_t}$  respectively for 2.5 and  $5 \mu\text{g}/\text{cm}^2$ ) compared to untreated cells ( $1.02 \cdot 2^{-\Delta\Delta C_t}$ ) (Figure 5(D)). All these results, therefore, suggest that the increase in cytoplasmic calcium levels induced by NiONPs may be related to altered TRPV4 channel activity.

#### **NiONPs impair intracellular calcium stores**

To investigate if a  $[\text{Ca}^{2+}]_i$  rise could also be mediated by intracellular  $\text{Ca}^{2+}$  stores, particularly by ER and mitochondria, intracellular calcium content was studied. In HPAEC after a 4 h-exposure to NiONPs ( $0.5\text{--}5 \mu\text{g}/\text{cm}^2$ ), a significant concentration-dependent increase in ER calcium levels and in mitochondria calcium levels was observed, respectively for  $0.5 \mu\text{g}/\text{cm}^2$  and for  $2.5 \mu\text{g}/\text{cm}^2$ , as compared to untreated cells (Figure 4(D,E)). These results, therefore, suggest that NiONPs can increase calcium levels in both organelles, further suggesting that these organelles may pump calcium from the cytoplasm.

#### **NiONPs induce mitochondria alterations**

Our results showed that NiONPs impair mitochondria with an increase in mitochondrial  $\text{O}_2^-$  production for  $2.5 \mu\text{g}/\text{cm}^2$  and with an increase in calcium mitochondrial levels (Figures 2(C) and 4(E)). The membrane mitochondrial potential ( $\Psi\text{MP}$ ) was then studied using the TMRM probe with confocal microscopy. As compared to controls, after a 4 h-exposure to NiONPs, both the  $\Psi\text{MP}$  (89.98%) (Figure 6(A)) and the mitochondrial mass decreased significantly for  $0.5 \mu\text{g}/\text{cm}^2$  (85.59%) (Figure 6(B)) as compared to untreated cells. In Figure 6(C), after HPAEC exposition to NiONPs, mitochondria seemed fragmented (white arrow), as compared to control cells.

#### **NiONPs increase apoptosis in HPAEC**

After a 24 h-exposure to NiONPs ( $0.5\text{--}10 \mu\text{g}/\text{cm}^2$ ), a significant and concentration-dependent increase in the number of apoptotic HPAEC was detected (29.32% and 38.34% respectively for 7.5 and  $10 \mu\text{g}/\text{cm}^2$ ), as compared to untreated cells (Figure 7(A)).

This increased HPAEC apoptosis was then confirmed by the significant decrease in bcl-2 mRNA expression, as assessed by RT-qPCR ( $0.36 \cdot 2^{-\Delta\Delta C_t}$ ), after a 24 h-exposure to NiONPs compared to control cells ( $1.05 \cdot 2^{-\Delta\Delta C_t}$ ) (Figure 7(B)).

#### **NiONPs impair NO production and increase the production of nitrites and nitrates**

The production of NO was measured using the DAF-FM probe with confocal microscopy, and the Griess reaction was used to determine reactive nitrosamine species such as peroxynitrites ( $\text{ONOO}^-$ ). After a 4 h-exposure of HPAEC to NiONPs ( $0.5\text{--}5 \mu\text{g}/\text{cm}^2$ ), a significant increase in NO production was observed (111.15%, 111.16%, and 109.83%, respectively for 0.5, 2.5, and  $5 \mu\text{g}/\text{cm}^2$ ) as compared to untreated cells (Figure 7(C)). Interestingly, after a 24 h-exposure to NiONPs ( $0.5\text{--}5 \mu\text{g}/\text{cm}^2$ ), a significant dose-dependent decrease of NO production was observed (78.49% and 68.60% respectively for 2.5 and  $5 \mu\text{g}/\text{cm}^2$ ) as compared to untreated cells (Figure 7(D)). We have previously shown that after a 4 h-exposure, NiONPs are able to increase intracellular production of  $\text{O}_2^-$  ( $2.5 \mu\text{g}/\text{cm}^2$ ) in HPAEC. Since NO can be oxidized by  $\text{O}_2^-$  to form NO metabolites such as  $\text{ONOO}^-$ , the production of nitrites and nitrates were then investigated in HPAEC. Our results showed that after a 24 h-exposure to NiONPs ( $0.5\text{--}5 \mu\text{g}/\text{cm}^2$ ), a significant increase of NO metabolites production was observed for  $5 \mu\text{g}/\text{cm}^2$  (0.77 ng/ $\mu\text{L}$ ), as compared to untreated cells (0.62 ng/ $\mu\text{L}$ ) (Figure 7(E)).

#### **NiONPs increase endothelin-1 production**

The production of ET-1, was measured by ELISA assay. After a 24 h-exposure of HPAEC to NiONPs ( $0.5\text{--}5 \mu\text{g}/\text{cm}^2$ ), a significant increase of ET-1 production was observed at the highest concentration of  $5 \mu\text{g}/\text{cm}^2$  (110.14 pg/mL of proteins) as compared to untreated cells (65.03 pg/mL of proteins) (Figure 7(F)). That result suggests that NiONPs may induce alterations in vascular reactivity.

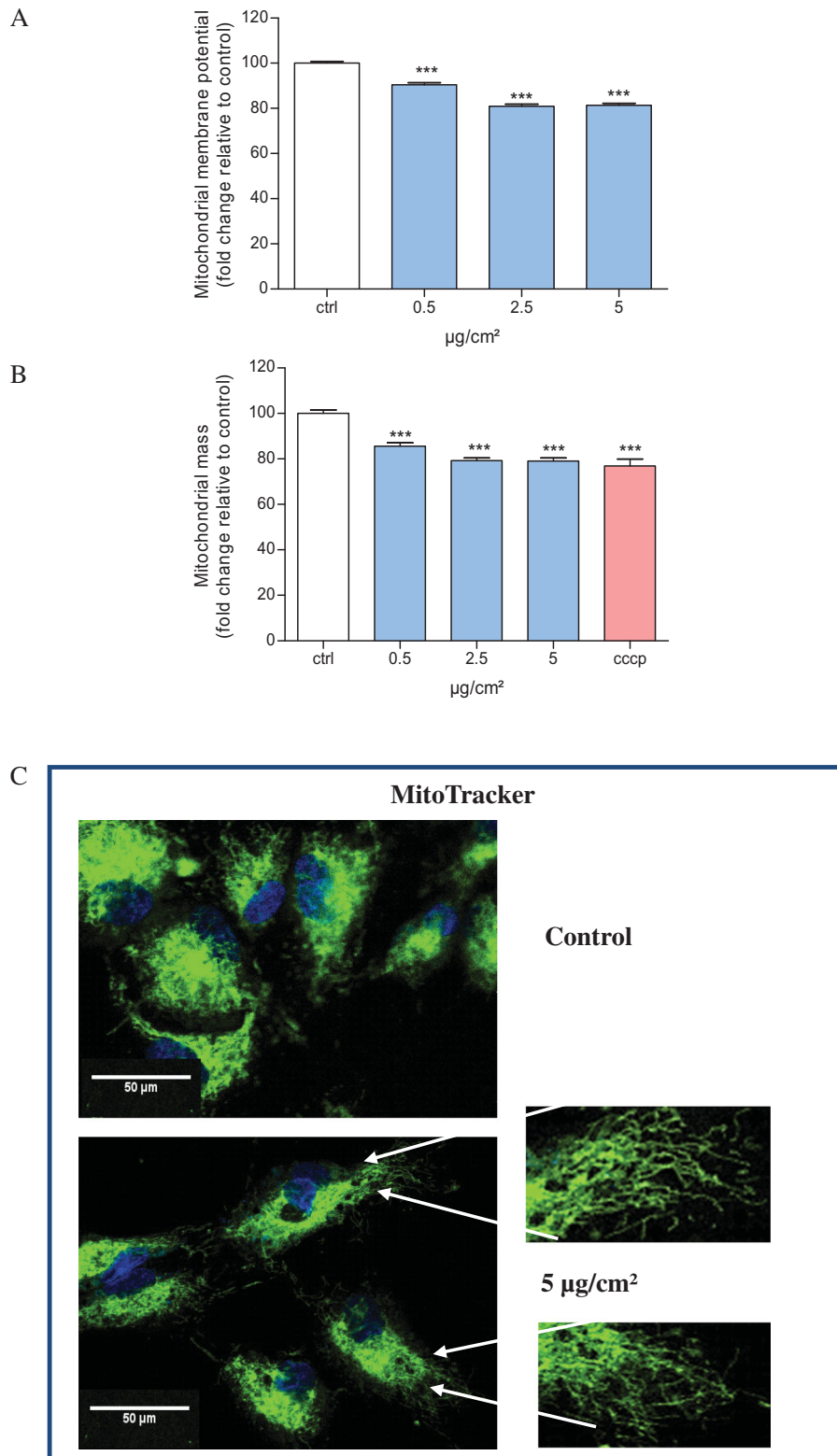


**Figure 6.** Mitochondria alteration after 4 h-exposure with NiONPs (0.5–5  $\mu\text{g}/\text{cm}^2$ ). (A) Mitochondrial potential membrane ( $\Psi_{\text{MP}}$ ) measured by confocal microscopy with TMRM probe (100 nM). (B) The mitochondrial mass measured by confocal microscopy with Mitotracker probe (1  $\mu\text{M}$ ). The values were normalized to the untreated cells and results were expressed as the fold change of the TMRM or Mitotracker probes fluorescence intensity relative to the control cells (100%). Data were mean  $\pm$  SEM of three independent experiments, ( $n = 3$ ) (six wells/concentration). Statistically significant at  $p < 0.001$ (\*\*\*) as compared to untreated control cells.

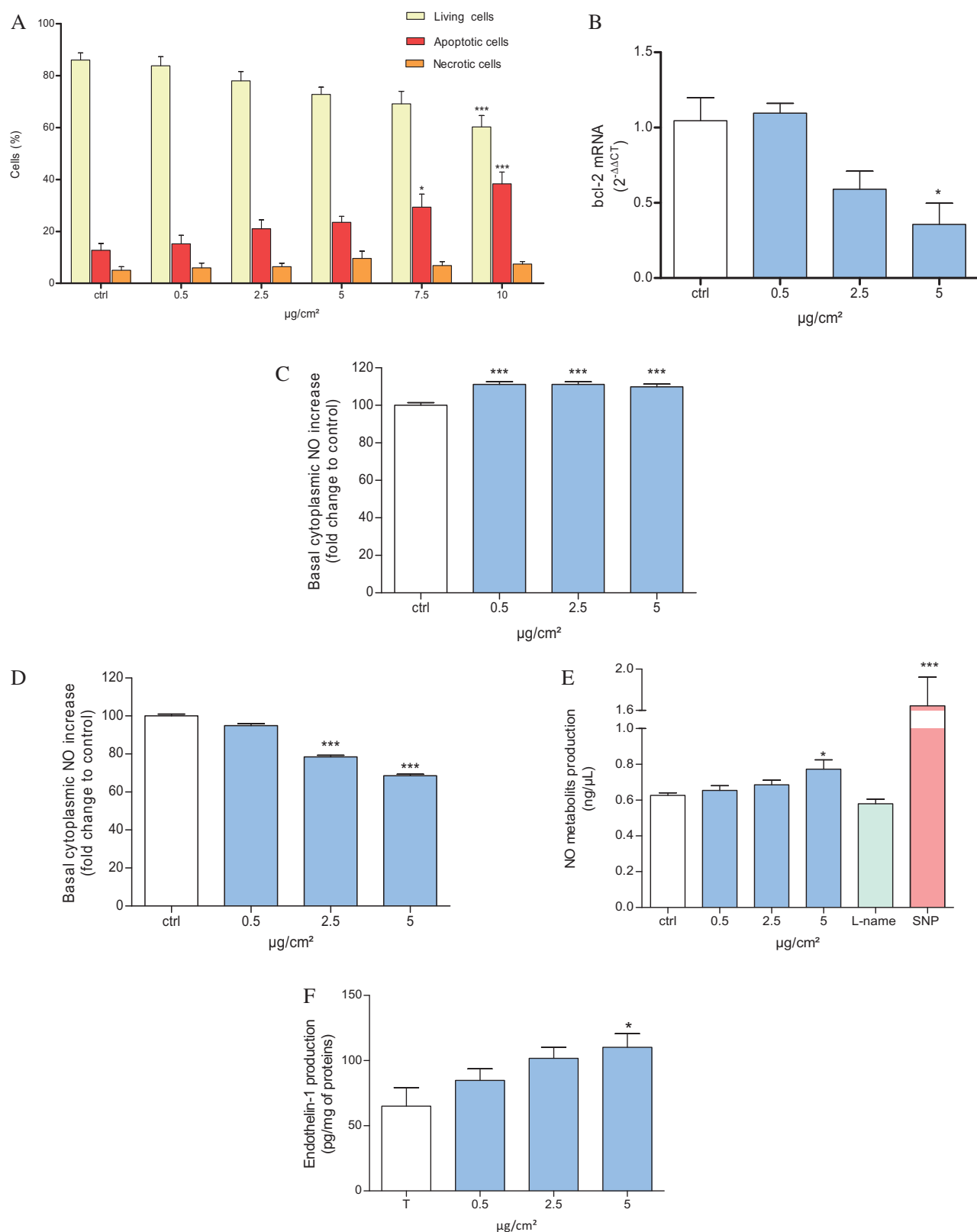


**Figure 7.** (A) Apoptotic and necrotic cells measured by Annexin V/PI assay after 24 h-exposure with NiONPs (0.5–10  $\mu\text{g}/\text{cm}^2$ ). Results were expressed as percentage relative to control cells. Data are Mean  $\pm$  SEM of four independent experiments ( $n = 4$ ), (eight wells/concentration). (B) bcl-2 mRNA expression in HPAEC after 24 h-exposure with NiONPs (0.5–5  $\mu\text{g}/\text{cm}^2$ ), measured by RT-qPCR. The results were expressed as the fold change of bcl-2 mRNA expression relative to the control cells. NO level was measured by confocal microscopy with DAF-FM probe (5  $\mu\text{M}$ ). (C) NO production after 4 h-exposure with NiONPs (0.5–5  $\mu\text{g}/\text{cm}^2$ ). (D) NO production after 24 h-exposure with NiONPs (0.5–5  $\mu\text{g}/\text{cm}^2$ ). The values were normalized to untreated cells, and results are

#### Figure 7. (Continued)

expressed as the fold change of DAF-FM probe fluorescence intensity relative to control cells. (E)  $\text{NO}_2^-$  and  $\text{NO}_3^-$  production measured by the Griess reaction after 24 h-exposure with NiONPs ( $0.5\text{--}5\text{ }\mu\text{g}/\text{cm}^2$ ). The results were expressed in  $\text{ng}/\mu\text{L}$ . Data were mean  $\pm$  SEM of four independent experiments, ( $n = 4$ ) (three wells/concentration). (F) ET-1 production in HPAEC after 24 h-exposure with NiONPs ( $0.5\text{--}5\text{ }\mu\text{g}/\text{cm}^2$ ). Production of ET-1 measured by ELISA assay. The results were expressed as  $\text{pg}/\text{mg}$  of proteins. Data were mean  $\pm$  SEM of five independent experiments,  $n = 5$  (three wells/concentration). Statistically significant at  $p < 0.05$  (\*) as compared to untreated control cells. Statistically significant at  $p < 0.05$  (\*),  $p < 0.01$  (\*\*),  $p < 0.001$  (\*\*\*) and  $p < 0.0001$  (\*\*\*\*), as compared to untreated control cells.

## Discussion

Occupational exposure in manufacturing and nickel laterite mines exploitations in New Caledonia could be a concern not only for workers handling NiONPs, but also for the surrounding population [ATSDR, 2005]. It is well-known that calcium has a key role in endothelial regulation and that alterations of calcium homeostasis can play a pathophysiological role in vascular diseases (Berridge, Bootman, and Roderick 2003). However, although only a few studies have investigated the direct effects of NiONPs on bronchial (BEAS-2B) and alveolar (A549) epithelial cells, their effects on pulmonary arterial endothelial cells remain unknown. Indeed, *in vitro* studies using human bronchial and alveolar epithelial cells have demonstrated the cytotoxicity of NiONPs, leading to a decrease in cell viability after exposure to  $0.1\text{--}40\text{ }\mu\text{g}/\text{cm}^2$ . Moreover, the same studies have shown that NiONPs ( $0.5\text{--}100\text{ }\mu\text{g}/\text{mL}$ ) generate oxidative stress, with an increase in the global ROS production and a decreased activity of antioxidant enzymes such as SOD, CAT, and glutathione (GSH) (Ahamed 2011; Mohamed et al. 2018; Duan et al. 2015; Latvala et al. 2016). Additionally, exposure to NiONPs ( $20\text{--}100\text{ }\mu\text{g}/\text{mL}$ ) leads to an increased secretion of pro-inflammatory cytokines, such as IL-6 and IL-8 in both types of epithelial cells (Capasso, Camatini, and Gualtieri 2014). The underlying cellular and molecular mechanisms remain unclear, in particular on calcium signaling and mitochondrial dysfunction.

Our results showed that polydispersed NiONPs suspension in the culture medium contained three types of population: (1) very large aggregates, (2) small aggregates, and (3) a large number of isolated particles (90% of the population) (Figure 1(B)). In acellular conditions, NiONPs were able to induce the generation of ROS in the culture medium (data not shown), probably due to their high surface reactivity. When HPAEC were exposed to NiONPs,

these particles were rapidly internalized in the cytoplasm into vesicles to form aggregates of different sizes. Despite the fact that NiONPs were not seen in mitochondria, some aggregates were detected very close to them, suggesting that they may be able to interfere with mitochondrial functions (Figure 1). Like other metallic NPs, NiONPs internalization appears to be a key factor in their toxicity (Munoz and Costa 2012). The cytotoxic effect of NiONPs on HPAEC was evaluated to select the concentrations (mortality rate  $< 30\%$ ) to be used for further mechanistic experiments. Taking into account the respiratory rate for a healthy man ( $20\text{ L}/\text{min.}$ , 12-h/day exposure), the alveolar deposits ( $20\text{--}50\%$ ), the alveolar surface ( $75\text{ m}^2$ ), and the possible internalization of the nanoparticles in endothelial cells, the different NiONPs concentrations used in this study ( $0.5\text{--}5\text{ }\mu\text{g}/\text{cm}^2$ ) would reflect an atmospheric exposure of approximately  $50\text{ ng}/\text{m}^3$ . These later NiONPs concentrations are realistic concentrations close to the ones found from particles exposure in New Caledonia near nickel laterite mines [Scal'AIR, 2018] (Akerlund et al. 2019). It was shown that one of the key mechanisms leading to metal oxide NPs cytotoxicity is an overproduction of ROS (Ivask et al. 2015). Our results demonstrate that NiONPs increased the global production of ROS in HPAEC along with a large increase in cytoplasmic  $\text{O}_2^-$  (Figure 2(B–D)). Transition metals, such as nickel, are known to produce reactive free radicals, such as  $\text{O}_2^-$ , via the Fenton reaction (Abdal Dayem et al. 2017). Previous studies carried out on A549 cells have shown a significant increase in ROS production after a 24 h-exposure to NiONPs (Mohamed et al. 2018). Our present study suggests that HPAEC may be more sensitive to NiONPs than epithelial cells, being able to produce ROS after a 4 h-exposure to NiONPs, only.

Once ROS are produced, the antioxidant system increases the production of antioxidant enzymes in



order to maintain the redox balance (Sies, Berndt, and Jones 2017). Thus, we assessed the effect of NiONPs exposure on the antioxidant response in HPAEC and our results showed a decrease in SOD activity (Figure 2(E)). Several authors have demonstrated that other NPs (i.e. silicon nanoparticles, carbon nanotubes) also decrease antioxidant enzyme activity in other types of endothelial cells, such as in human umbilical vein endothelial cells (HUVECs) (Cao et al. 2017). These enzymes undergo functional changes by direct interactions with NPs (Zhang et al. 2019). A decrease in the antioxidant activity might explain the NiONPs-induced oxidative stress in HPAEC. It has been demonstrated, both *in vivo* and *in vitro*, that many metallic oxide NPs generate ROS. An enhanced ROS generation might activate the inflammatory pathways via the secretion of pro-inflammatory cytokines (Zhang et al. 2012). Our results are in accordance with that previous study. We showed that NiONPs can induce a pro-inflammatory response, characterized by both increased IL-6 expression and secretion (Figure 3). Similar results have already been observed in HPAEC after exposure to Ultrafine Particles (<100 nm) (Karoly et al. 2007). We also showed that this pro-inflammatory response was strongly reduced by a pretreatment with antioxidant enzymes, such as PEG-SOD and PEG-CAT. Therefore, we hypothesize that the NiONPs-induced pro-inflammatory response might be closely related to oxidative stress, a relationship often highlighted after NP exposure (Nel et al. 2006). In addition, there is evidence that oxidative stress contributes to the pathophysiology of vascular diseases, along with inflammation, which plays an important role in cardiovascular diseases (Rafikova, Al Ghoulleh, and Rafikov 2019).

Given the importance of calcium signaling in endothelial dysfunction, the effect of NiONPs exposure on calcium signaling was evaluated in HPAEC. NiONPs increased the basal calcium level, in a concentration-dependent manner (Figure 4(A,B)). This observation is in line with the previously published data after NiONPs exposure on BEAS-2B cells (DI Bucchianico et al. 2018). Moreover, it seems important to determine whether the  $[Ca^{2+}]_i$  increase came from intracellular calcium stocks (such as ER) and/or from the extracellular source, especially via the calcium membrane channels disturbance. Our current finding of  $[Ca^{2+}]_i$  rise being significantly reduced

after NiONPs exposure in the absence of extracellular calcium, is strong evidence in favor of the second hypothesis. In addition, TRPV4 channel activity was reduced and, by blocking that TRPV4 channel activity with an antagonist, no calcium homeostasis alteration was then observed. Regarding the implication of intracellular calcium stores, an increase in  $[Ca^{2+}]_{ER}$  was observed. Indeed, ER also acts as a calcium buffer site that regulates intracellular calcium homeostasis (Marchi et al. 2018). All of the results can be explained by the membrane calcium channel alterations. Indeed, a previous study has shown that metallic oxide NPs, that is, CeONPs, can interact with the membrane calcium channels (Xiang et al. 2016). Stretch-activated channels are particularly involved in the calcium influx of vascular cells, and they might be a target site of NPs. Previous studies have shown that silica NPs interact with TRPV channels in airway epithelial cells by specifically inhibiting TRPV4. The later interaction is responsible for physiological dysfunctions in the respiratory tract of mice (Sanchez et al. 2017). Likewise, our findings suggest that NiONPs interact with TRPV4 channels (Figure 5).

It is interesting to note that  $[Ca^{2+}]_i$  rise differs according to the type of particles as well as their size and their physicochemical characteristics. Indeed, in A549 cells,  $NiCl_2$  (20  $\mu M$ ), increases calcium release from intracellular calcium stores (Cortijo et al. 2010), such as in HPAEC after carbon black NPs exposure (Deweirdt et al. 2020). Another study in rat pulmonary artery smooth muscle cells shows that  $SiO_2$  NPs exposure, increases  $[Ca^{2+}]_i$  originating from both extracellular and intracellular calcium sources, with an implication of TRPV (Dubes et al. 2017). All these results suggest that metallic NPs physicochemical characteristics are important in calcium signaling alteration in different vascular cells, mainly through alterations of membrane calcium channels.

$[Ca^{2+}]_i$  homeostasis alteration may originate from oxidative stress (Gordeeva, Zvyagilskaya, and Labas 2003). In a previous study on HPAEC, we showed that carbon black NPs (13 nm)-induced alteration in intracellular calcium homeostasis was closely related to oxidative stress (Deweirdt et al. 2020). In this previous study, the  $[Ca^{2+}]_i$  rise was also reduced by pretreatment with antioxidant enzymes, as observed in this present study with NiONPs.

$\text{Ca}^{2+}$  : Calcium  
 IL-6 : Interleukin-6  
 SOD : Superoxide Dismutase  
 CAT : Catalase  
 TRPV4 : transient receptor potential vanilloid 4  
 NO : Nitrogen oxygen  
 $\text{H}_2\text{O}_2$  : Hydrogen peroxide  
 $\text{O}_2^-$  : Superoxide anion  
 HPAEC : Human pulmonary artery endothelial cell  
 $\Psi\text{MP}$  : Mitochondrial membrane potential  
 NPsNiO : Nickel oxide nanoparticles  
 ET-1 : Endothelin-1

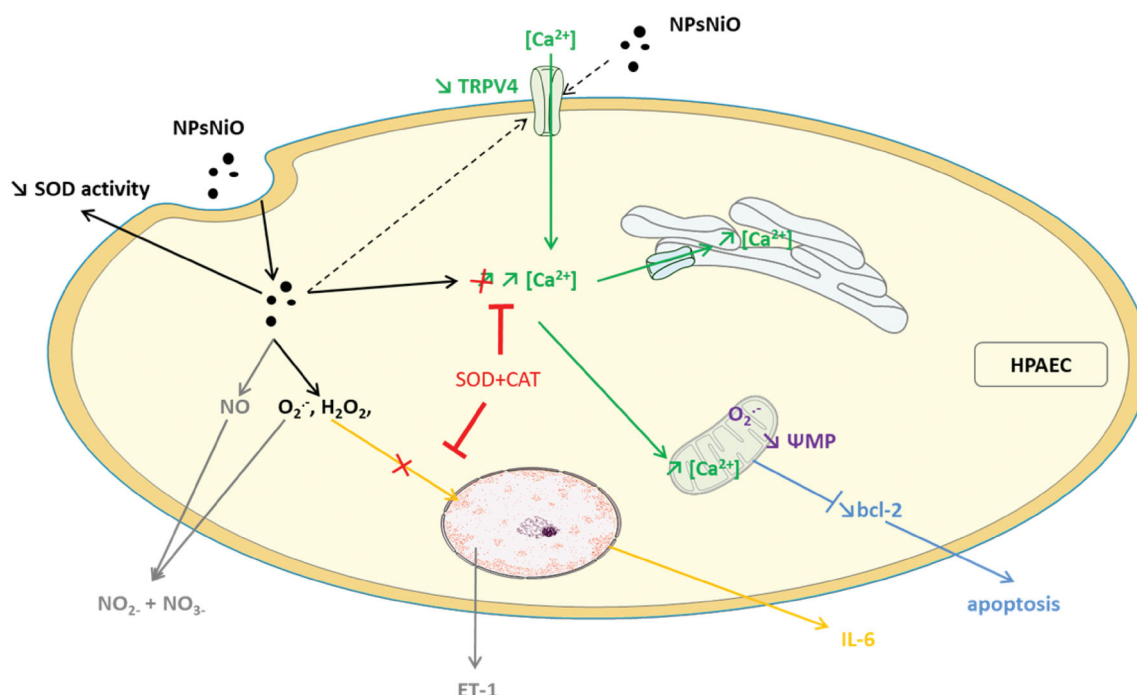


**Figure 8.** Summary of main results. NPsNiO caused damages that was dependent on oxidative stress and mitochondrial dysfunction.

However, such pretreatment did not fully restore calcium homeostasis thus indicating that oxidative stress was not the only mechanism responsible.

NiONPs could also alter mitochondrial function, especially because of the localization of NiONPs in the cytoplasm near the mitochondria, because of the importance of oxidative stress implication, and of the disruption of calcium homeostasis. Indeed, ROS, such as  $\text{O}_2^-$  may induce mitochondrial membrane lipoperoxidation, leading to the impairment of mitochondrial membrane potential. The later alterations can dysregulate the mitochondrial respiratory chain, the  $\beta$ -oxidation, or induce apoptosis (Prakash, Pabelick, and Sieck 2017). In the current study, a disruption of mitochondrial activity after NiONPs exposure was highlighted with: (i) an overproduction of mitochondrial  $\text{O}_2^-$ ; (ii) a  $[\text{Ca}^{2+}]_m$

rise; (iii) a decrease in mitochondrial membrane potential and (iv) a decrease in mitochondrial mass (Figures 2 and 4 and Figure 6). Then, the apoptosis was evaluated and our results showed an increase in apoptotic cell number (Figure 7(A,B)). Apoptosis has previously been detected in BEAS-2B cells and in HUVECs, after exposures to NiONPs and SiNPs (Duan et al. 2015; Guo et al. 2018). Moreover, the decrease of anti-apoptotic factor bcl-2 expression observed in HPAEC after NiONPs exposure confirmed involvement of the apoptosis pathway. Interestingly, an alteration of bcl-2 expression was also observed in BEAS-2B after titanium oxide NPs exposure (Shi et al. 2010). The present results demonstrate that the main mechanism of cell death after NiONPs exposure involves mitochondria alteration-mediated apoptosis, which could lead to

endothelial dysfunction causing pulmonary vascular diseases (Chambers, Rounds, and Lu 2018). Another study also reports that cardiovascular diseases are associated with mitochondrial impairment (Chistiakov et al. 2018).

Finally, NO plays an important vasculoprotective role regulated by calcium concentration. Based on our results regarding NiONPs-induced homeostasis calcium alteration, we decided to further study NO production. Moreover, it is well known that the unstable  $O_2^-$  can react with NO. After a 4 h-exposure to NiONPs, an increase of NO production was observed in HPAEC (Figure 7(C)). However, after a 24 h-exposure a decrease of NO production was noticed. The decrease in NO bioavailability might be explained by a rapid kinetic reaction between NO and  $O_2^-$  to form metabolites such as peroxynitrites. The later toxic molecules may be involved in the aggravation of cardiovascular diseases (Pacher, Beckman, and Liaudet 2007). Consequently, the production of NO metabolites (i.e. nitrites, nitrates), which reflects the peroxynitrites production, was analyzed. Our results showed a significant increase in NO metabolites. Furthermore, after a 24 h-exposure to NiONPs, we detected a significant increase in ET-1 which is a mediator of vasoconstriction. Production of NO toxic metabolites associated with the decrease of NO bioavailability and the increase in ET-1 production could result in an imbalance between relaxation/contraction of smooth muscle cells in favor of contraction resulting in an altered vascular reactivity state, one of the critical events involved in PH (Billaud et al. 2009).

Our results are summarized in Figure 8.

## Conclusion

The present study shows that NiONPs primarily induce an intracellular ROS overproduction in HPAEC, leading to a pro-inflammatory response and a  $[Ca^{2+}]_i$  rise. Disruption of intracellular calcium homeostasis can be explained by alterations of membrane calcium channels, particularly the TRPV4 channels, and at least in part by oxidative stress. In addition, NiONPs trigger endothelial toxicity through mitochondrial dysfunction which is characterized by (1) mitochondrial ROS generation, (2) mitochondrial membrane potential alteration, and (3) mitochondrial calcium overload. Furthermore,

we have demonstrated that NiONPs induce endothelial apoptosis as a result of their toxic effects. Finally, the decrease in NO bioavailability may contribute to an alteration of the vascular reactivity and to endothelial dysfunction, which are both critical pathophysiological mechanisms underlying many vascular diseases. Thus, one can assume that the workers and the population exposed to NiONPs in New Caledonia may be at risk to develop exacerbation of preexisting vascular diseases.

## Acknowledgments

The authors thank Ms. C. Freund-Chapellier for her constructive remarks on the linguistic content of the manuscript.

## Disclosure statement

No potential conflict of interest was reported by the author(s).

## Funding

The author(s) reported there is no funding associated with the work featured in this article.

## ORCID

Magalie Baudrimont  <http://orcid.org/0000-0001-9901-8435>

## References

- Abdal Dayem, A., M. K. Hossain, S. B. Lee, K. Kim, S. K. Saha, G. M. Yang, H. Y. Choi, and S. G. Cho. 2017. "The Role of Reactive Oxygen Species (ROS) in the Biological Activities of Metallic Nanoparticles." *International Journal of Molecular Sciences* 18 (1): 120.
- Ahamed, M. 2011. "Toxic Response of Nickel Nanoparticles in Human Lung Epithelial A549 Cells." *Toxicology in Vitro* 25 (4): 930–936.
- Akerlund, E., M. S. Islam, S. Mccarrick, E. Alfaro-Moreno, and H. L. Karlsson. 2019. "Inflammation and (Secondary) Genotoxicity of Ni and NiO Nanoparticles." *Nanotoxicology* 13 (8): 1060–1072.
- Andersen, I., and K. B. Svenes. 1989. "Determination of Nickel in Lung Specimens of Thirty-Nine Autopsied Nickel Workers." *International Archives of Occupational and Environmental Health* 61 (4): 289–295.
- Berridge, M. J., M. D. Bootman, and H. L. Roderick. 2003. "Calcium Signalling: Dynamics, Homeostasis and Remodelling." *Nature Reviews. Molecular Cell Biology* 4 (7): 517–529.

- Billaud, M., R. Marthan, J. P. Savineau, and C. Guibert. 2009. "Vascular Smooth Muscle Modulates Endothelial Control of Vasoreactivity via Reactive Oxygen Species Production through Myoendothelial Communications." *PLoS One* 4 (7): e6432.
- Cao, Y., Y. Gong, L. Liu, Y. Zhou, X. Fang, C. Zhang, Y. Li, and J. Li. 2017. "The Use of Human Umbilical Vein Endothelial Cells (HUVECs) as an in Vitro Model to Assess the Toxicity of Nanoparticles to Endothelium: A Review." *Journal of Applied Toxicology* 37 (12): 1359–1369. doi:10.1002/jat.3470.
- Capasso, L., M. Camatini, and M. Gualtieri. 2014. "Nickel Oxide Nanoparticles Induce Inflammation and Genotoxic Effect in Lung Epithelial Cells." *Toxicology Letters* 226 (1): 28–34.
- Chambers, E., S. Rounds, and Q. Lu. 2018. "Pulmonary Endothelial Cell Apoptosis in Emphysema and Acute Lung Injury." *Advances in Anatomy, Embryology, and Cell Biology* 228: 63–86.
- Chang, X. H., A. Zhu, F. F. Liu, L. Y. Zou, L. Su, S. K. Liu, H. H. Zhou, et al. 2017. "Nickel Oxide Nanoparticles Induced Pulmonary Fibrosis via TGF- $\beta$ 1 Activation in Rats." *Human & Experimental Toxicology* 36 (8): 802–812.
- Chen, X., Z. Zhong, Z. Xu, L. Chen, and Y. Wang. 2010. "2',7'-Dichlorodihydrofluorescein as a Fluorescent Probe for Reactive Oxygen Species Measurement: Forty Years of Application and Controversy." *Free Radical Research* 44 (6): 587–604.
- Chistiakov, D. A., T. P. Shkurat, A. A. Melnichenko, A. V. Grechko, and A. N. Orekhov. 2018. "The Role of Mitochondrial Dysfunction in Cardiovascular Disease: A Brief Review." *Annals of Medicine* 50 (2): 121–127.
- Cortijo, J., J. Milara, M. Mata, E. Donet, N. Gavara, S. E. Peel, I. P. Hall, and E. J. Morcillo. 2010. "Nickel Induces Intracellular Calcium Mobilization and Pathophysiological Responses in Human Cultured Airway Epithelial Cells." *Chemico-Biological Interactions* 183 (1): 25–33.
- Courtois, A., P. Andujar, Y. Ladeiro, T. Ducret, F. Rogerieux, G. Lacroix, I. Baudrimont, et al. 2010. "Effect of Engineered Nanoparticles on Vasomotor Responses in Rat Intrapulmonary Artery." *Toxicology and Applied Pharmacology* 245 (2): 203–210.
- Deweirdt, J., J. F. Quignard, B. Crobeddu, A. Baeza-Squiban, J. Sciare, A. Courtois, S. Lacomme, et al. 2017. "Involvement of Oxidative Stress and Calcium Signaling in Airborne Particulate Matter - Induced Damages in Human Pulmonary Artery Endothelial Cells." *Toxicology in Vitro* 45 (3): 340–350.
- Deweirdt, J., J. F. Quignard, S. Lacomme, E. Gontier, S. Mornet, J. P. Savineau, R. Marthan, C. Guibert, and I. Baudrimont. 2020. "In Vitro Study of Carbon Black Nanoparticles on Human Pulmonary Artery Endothelial Cells: Effects on Calcium Signaling and Mitochondrial Alterations." *Archives of Toxicology* 94 (7): 2331–2348. doi:10.1007/s00204-020-02764-9.
- DI Bucchianico, S., A. R. Gliga, E. Akerlund, S. Skoglund, I. O. Wallinder, B. Fadeel, and H. L. Karlsson. 2018. "Calcium-Dependent Cyto- and Genotoxicity of Nickel Metal and Nickel Oxide Nanoparticles in Human Lung Cells." *Particle and Fibre Toxicology* 15 (1): 32.
- Dikalov, S. I., I. A. Kirilyuk, M. Voinov, and I. A. Grigor'Ev. 2011. "EPR Detection of Cellular and Mitochondrial Superoxide Using Cyclic Hydroxylamines." *Free Radical Research* 45 (4): 417–430.
- Duan, W. X., M. D. He, L. Mao, F. H. Qian, Y. M. Li, H. F. Pi, C. Liu, et al. 2015. "NiO Nanoparticles Induce Apoptosis through Repressing SIRT1 in Human Bronchial Epithelial Cells." *Toxicology and Applied Pharmacology* 286 (2): 80–91.
- Dubes, V., T. Parpaite, T. Ducret, J. F. Quignard, S. Mornet, N. Reinhardt, I. Baudrimont, et al. 2017. "Calcium Signalling Induced by in Vitro Exposure to Silicon Dioxide Nanoparticles in Rat Pulmonary Artery Smooth Muscle Cells." *Toxicology* 375: 37–47.
- Ducret, T., J. EL Arrouchi, A. Courtois, J. F. Quignard, R. Marthan, and J. P. Savineau. 2010. "Stretch-Activated Channels in Pulmonary Arterial Smooth Muscle Cells from Normoxic and Chronically Hypoxic Rats." *Cell Calcium* 48 (5): 251–259.
- Filippini, A., A. D'Amore, and A. D'Alessio. 2019. "Calcium Mobilization in Endothelial Cell Functions." *International Journal of Molecular Sciences* 20 (18): 4525.
- Gordeeva, A. V., R. A. Zvyagilskaya, and Y. A. Labas. 2003. "Cross-Talk between Reactive Oxygen Species and Calcium in Living Cells." *Biochemistry* 68 (10): 1077–1080.
- Goswami, C., J. Kuhn, P. A. Heppenstall, and T. Hucho. 2010. "Importance of Non-Selective Cation Channel TRPV4 Interaction with Cytoskeleton and Their Reciprocal Regulations in Cultured Cells." *PLoS One* 5 (7): e11654.
- Guibert, C., R. Marthan, and J. P. Savineau. 2007. "Modulation of Ion Channels in Pulmonary Arterial Hypertension." *Current Pharmaceutical Design* 13 (24): 2443–2455.
- Guo, C., R. Ma, X. Liu, Y. Xia, P. Niu, J. Ma, X. Zhou, Y. Li, and Z. Sun. 2018. "Silica Nanoparticles Induced Endothelial Apoptosis via Endoplasmic Reticulum Stress-Mitochondrial Apoptotic Signaling Pathway." *Chemosphere* 210: 183–192.
- He, Z. L., X. E. Yang, and P. J. Stoffella. 2005. "Trace Elements in Agroecosystems and Impacts on the Environment." *Journal of Trace Elements in Medicine and Biology* 19 (2–3): 125–140. doi:10.1016/j.jtemb.2005.02.010.
- Horemans, B., C. Van Holsbeke, W. Vos, L. Darchuk, V. Novakovic, A. C. Fontan, J. De Backer, R. Van Grieken, W. De Backer, and K. De Wael. 2012. "Particle Deposition in Airways of Chronic Respiratory Patients Exposed to an Urban Aerosol." *Environmental Science & Technology* 46 (21): 12162–12169. doi:10.1021/es302755s.
- Imran Din, M., and A. Rani. 2016. "Recent Advances in the Synthesis and Stabilization of Nickel and Nickel Oxide Nanoparticles: A Green Adeptness." *International Journal of Analytical Chemistry* 2016: 1–14. doi:10.1155/2016/3512145.
- Isnard, S., L. L'Huillier, F. Rigault, and T. Jaffré. 2016. "How Did the Ultramafic Soils Shape the Flora of the New



- Caledonian Hotspot?" *Plant and Soil* 403 (1–2): 53–76. doi:10.1007/s11104-016-2910-5.
- Ivask, A., T. Titma, M. Visnapuu, H. Vija, A. Kakinen, M. Sihtmae, S. Pokhrel, et al. 2015. "Toxicity of 11 Metal Oxide Nanoparticles to Three Mammalian Cell Types in Vitro." *Current Topics in Medicinal Chemistry* 15 (18): 1914–1929.
- Karoly, E. D., Z. Li, L. A. Dailey, X. Hyseni, and Y. C. Huang. 2007. "Up-Regulation of Tissue Factor in Human Pulmonary Artery Endothelial Cells after Ultrafine Particle Exposure." *Environmental Health Perspectives* 115 (4): 535–540. doi:10.1289/ehp.9556.
- Konczol, M., E. Goldenberg, S. Ebeling, B. Schafer, M. Garcia-Kaufer, R. Gminski, B. Grobety, et al. 2012. "Cellular Uptake and Toxic Effects of Fine and Ultrafine Metal-Sulfate Particles in Human A549 Lung Epithelial Cells." *Chemical Research in Toxicology* 25 (12): 2687–2703.
- Lai, N., W. Lu, and J. Wang. 2015. "Ca(2+) and Ion Channels in Hypoxia-Mediated Pulmonary Hypertension." *International Journal of Clinical and Experimental Pathology* 8 (2): 1081–1092.
- Latvala, S., J. Hedberg, S. Di Bucchianico, L. Moller, I. Odnevall Wallinder, K. Elihn, and H. L. Karlsson. 2016. "Nickel Release, ROS Generation and Toxicity of Ni and NiO Micro- and Nanoparticles." *PLoS One* 11 (7): e0159684.
- Losfeld, G., L. L'Huillier, B. Fogliani, T. Jaffre, and C. Grison. 2015. "Mining in New Caledonia: Environmental Stakes and Restoration Opportunities." *Environmental Science and Pollution Research International* 22 (8): 5592–5607.
- Marchi, S., S. Patergnani, S. Missiroli, G. Morciano, A. Rimessi, M. R. Wieckowski, C. Giorgi, and P. Pinton. 2018. "Mitochondrial and Endoplasmic Reticulum Calcium Homeostasis and Cell Death." *Cell Calcium* 69: 62–72.
- Miller, M. R., J. B. Raftis, J. P. Langrish, S. G. Mclean, P. Samutrtai, S. P. Connell, S. Wilson, et al. 2017. "Inhaled Nanoparticles Accumulate at Sites of Vascular Disease." *ACS Nano* 11 (5): 4542–4552. doi:10.1021/acsnano.6b08551.
- Mo, Y., M. Jiang, Y. Zhang, R. Wan, J. Li, C. J. Zhong, H. Li, S. Tang, and Q. Zhang. 2019. "Comparative Mouse Lung Injury by Nickel Nanoparticles with Differential Surface Modification." *Journal of Nanobiotechnology* 17 (1): 2.
- Mohamed, K., K. Zine, K. Fahima, E. Abdelfattah, S. M. Sharifudin, and K. Duduku. 2018. "NiO Nanoparticles Induce Cytotoxicity Mediated through ROS Generation and Impairing the Antioxidant Defense in the Human Lung Epithelial Cells (A549): Preventive Effect of Pistacia Lentiscus Essential Oil." *Toxicology Reports* 5: 480–488. doi:10.1016/j.toxrep.2018.03.012.
- Munoz, A., and M. Costa. 2012. "Elucidating the Mechanisms of Nickel Compound Uptake: A Review of Particulate and Nano-Nickel Endocytosis and Toxicity." *Toxicology and Applied Pharmacology* 260 (1): 1–16.
- Nel, A., T. Xia, L. Madler, and N. Li. 2006. "Toxic Potential of Materials at the Nanolevel." *Science* 311 (5761): 622–627.
- Nemmar, A., P. H. M. Hoet, B. Vanquickenborne, D. Dinsdale, M. Thomeer, M. F. Hoylaerts, H. Vanbilloen, L. Mortelmans, and B. Nemery. 2002. "Passage of Inhaled Particles into the Blood Circulation in Humans." *Circulation* 105 (4): 411–414.
- Norseth, T. 1994. "Environmental Pollution around Nickel Smelters in the Kola Peninsula (Russia)." *The Science of the Total Environment* 148 (2–3): 103–108.
- Oberdorster, G., E. Oberdorster, and J. Oberdorster. 2005. "Nanotoxicology: An Emerging Discipline Evolving from Studies of Ultrafine Particles." *Environmental Health Perspectives* 113: 823–839.
- Pacher, P., J. S. Beckman, and L. Liaudet. 2007. "Nitric Oxide and Peroxynitrite in Health and Disease." *Physiological Reviews* 87 (1): 315–424.
- Parpaite, T., G. Cardouat, M. Mauroux, J. Gillibert-Duplantier, P. Robillard, J. F. Quignard, R. Marthan, J. P. Savineau, and T. Ducret. 2016. "Effect of Hypoxia on TRPV1 and TRPV4 Channels in Rat Pulmonary Arterial Smooth Muscle Cells." *European Journal of Physiology* 468 (1): 111–130.
- Pasquet, C., P. Gunkel-Grillon, C. Laporte-Magoni, A. Serres, T. Quiniou, F. Rocca, F. Monna, R. Losno, F. Van Oort, and C. Chateau. 2016. "Alternative Dry Separation of PM10 from Soils for Characterization by Kinetic Extraction: Example of New Caledonian Mining Soils." *Environmental Science and Pollution Research International* 23 (24): 25105–25113.
- Prakash, Y. S., C. M. Pabelick, and G. C. Sieck. 2017. "Mitochondrial Dysfunction in Airway Disease." *Chest* 152 (3): 618–626.
- Rafikova, O., I. Al Ghoul, and R. Rafikov. 2019. "Focus on Early Events: Pathogenesis of Pulmonary Arterial Hypertension Development." *Antioxidants & Redox Signaling* 31 (13): 933–953.
- Sanchez, A., J. L. Alvarez, K. Demydenko, C. Jung, Y. A. Alpizar, J. Alvarez-Collazo, S. M. Cokic, M. A. Valverde, P. H. Hoet, and K. Talavera. 2017. "Silica Nanoparticles Inhibit the Cation Channel TRPV4 in Airway Epithelial Cells." *Particle and Fibre Toxicology* 14 (1): 43.
- Sandow, S. L., S. Senadheera, T. H. Grayson, D. G. Welsh, and T. V. Murphy. 2012. "Calcium and Endothelium-Mediated Vasodilator Signaling." *Advances in Experimental Medicine and Biology* 740: 811–831.
- Senoh, H., H. Kano, M. Suzuki, M. Ohnishi, H. Kondo, K. Takanobu, Y. Umeda, S. Aiso, and S. Fukushima. 2017. "Comparison of Single or Multiple Intratracheal Administration for Pulmonary Toxic Responses of Nickel Oxide Nanoparticles in Rats." *Journal of Occupational Health* 59 (2): 112–121. doi:10.1539/joh.16-0184-OA.
- Shi, Y., F. Wang, J. He, S. Yadav, and H. Wang. 2010. "Titanium Dioxide Nanoparticles Cause Apoptosis in BEAS-2B Cells through the Caspase 8/t-Bid-Independent Mitochondrial Pathway." *Toxicology Letters* 196 (1): 21–27.
- Sies, H., C. Berndt, and D. P. Jones. 2017. "Oxidative Stress." *Annual Review of Biochemistry* 86: 715–748.
- Sioutas, C., R. J. Delfino, and M. Singh. 2005. "Exposure Assessment for Atmospheric Ultrafine Particles (UFPs) and Implications in Epidemiologic Research." *Environmental Health Perspectives* 113 (8): 947–955. doi:10.1289/ehp.7939.



- St-Jean, A., Y. Barguil, Y. Dominique, L. E. B. Bot, P. Ayotte, and S. Cordier. 2018. "Nickel and Associated Metals in New Caledonia: Exposure Levels and Their Determinants." *Environment International* 118: 106–115.
- Xiang, J., J. Li, J. He, X. Tang, C. Dou, Z. Cao, B. Yu, et al. 2016. "Cerium Oxide Nanoparticle Modified Scaffold Interface Enhances Vascularization of Bone Grafts by Activating Calcium Channel of Mesenchymal Stem Cells." *ACS Applied Materials & Interfaces* 8 (7): 4489–4499.
- Ying, Z., X. Xu, M. Chen, D. Liu, M. Zhong, L. C. Chen, Q. Sun, and S. Rajagopalan. 2013. "A Synergistic Vascular Effect of Airborne Particulate Matter and Nickel in a Mouse Model." *Toxicological Sciences* 135 (1): 72–80. doi:[10.1093/toxsci/kft136](https://doi.org/10.1093/toxsci/kft136).
- Yokel, R. A., S. M. Lasley, and D. C. Dorman. 2006. "The Speciation of Metals in Mammals Influences Their Toxicokinetics and Toxicodynamics and Therefore Human Health Risk Assessment." *Journal of Toxicology and Environmental Health. Part B, Critical Reviews* 9 (1): 63–85.
- Zhang, R., C. Jia, L. Zhao, J. Pan, Q. Niu, and R. Liu. 2019. "Characterization of the Interaction between Carbon Black and Three Important Antioxidant Proteins Using Multi Spectroscopy and Modeling Simulations." *Chemosphere* 222: 823–830.
- Zhang, H., Z. Ji, T. Xia, H. Meng, C. Low-Kam, R. Liu, S. Pokhrel, et al. 2012. "Use of Metal Oxide Nanoparticle Band Gap to Develop a Predictive Paradigm for Oxidative Stress and Acute Pulmonary Inflammation." *ACS Nano* 6 (5): 4349–4368.
- Zheng, Y., B. Zhu, H. Chen, W. You, C. Jiang, and J. Yu. 2017. "Hierarchical Flower-like Nickel(II) Oxide Microspheres with High Adsorption Capacity of Congo Red in Water." *Journal of Colloid and Interface Science* 504: 688–696.